

NOAA Technical Memorandum OAR PMEL-117

Correcting Moored ADCP Data for Fish-Bias Errors at 0°, 110°W and 0°, 140°W from 1993 to 1995

Patricia E. Plimpton, H. Paul Freitag, and Michael J. McPhaden

Pacific Marine Environmental Laboratory
7600 Sand Point Way NE
Seattle, WA 98115

April 2000

Contribution 2104 from NOAA/Pacific Marine Environmental Laboratory

NOTICE

Mention of a commercial company or product does not constitute an endorsement by NOAA/OAR. Use of information from this publication concerning proprietary products or the tests of such products for publicity or advertising purposes is not authorized.

Contribution No. 2104 from NOAA/Pacific Marine Environmental Laboratory

For sale by the National Technical Information Service, 5285 Port Royal Road
Springfield, VA 22161

Contents

1.	Introduction	1
2.	Instrumentation and Data Processing	2
3.	ADCP Velocity Bias	5
4.	ADCP Data Correction	6
5.	Summary	8
6.	Acknowledgments	9
7.	References	9

List of Figures

1	Map of mooring locations for the Tropical Atmosphere Ocean (TAO) array	12
2	Schematic of PROTEUS mooring	13
3	Depth and time coverage of mechanical current meter data at 0°, 110°W	14
4	Depth and time coverage of mechanical current meter data at 0°, 140°W	15
5	Time series of ADCP-MCM speed difference and echo intensity range at 0°, 110°W	16
6	Time series of ADCP-MCM speed difference and echo intensity range at 0°, 140°W	17
7	Profiles of mean speed and direction differences for PR13	18
8	Profiles of mean speed and direction differences for PR14	19
9	Profiles of mean speed and direction differences for PR15	20
10	Profiles of mean speed and direction differences for PR16	21
11	Profiles of mean speed and direction differences for PR17	22
12	Profiles of mean speed and direction differences for PR18	23
13	Profiles of mean speed and direction differences for PR19	24
14	Profiles of mean speed and direction differences for PR20	25
15	The first three EOF eigenvectors and time series of ADCP-MCM speed differences for PR13	26
16	The first three EOF eigenvectors and time series of ADCP-MCM speed differences for PR14	27
17	The first three EOF eigenvectors and time series of ADCP-MCM speed differences for PR15	28
18	The first three EOF eigenvectors and time series of ADCP-MCM speed differences for PR16	29
19	The first three EOF eigenvectors and time series of ADCP-MCM speed differences for PR17	30
20	The first three EOF eigenvectors and time series of ADCP-MCM speed differences for PR18	31
21	The first three EOF eigenvectors and time series of ADCP-MCM speed differences for PR19	32
22	The first three EOF eigenvectors and time series of ADCP-MCM speed differences for PR20	33
23	Zonal and meridional velocity at 0°, 110°W from corrected daily profiles of ADCP data	34

24	Zonal and meridional velocity at 0°, 140°W from corrected daily profiles of ADCP data	35
----	---	----

List of Tables

1	PROTEUS mooring deployments at 0°, 110°W and 0°, 140°W. . . .	3
2	Comparison statistics between existing speeds and speeds computed with multiple linear regression formulae	4
3	Percent variance corrected for each of the first three vertical modes and their total for each deployment.	7

Correcting Moored ADCP Data for Fish-Bias Errors at 0° , 110°W and 0° , 140°W from 1993 to 1995

Patricia E. Plimpton, H. Paul Freitag, and Michael J. McPhaden

Abstract. Moorings in the Tropical Atmosphere Ocean (TAO) array monitor upper ocean velocity, temperature, and salinity as well as atmospheric parameters. Beginning in 1990, PROTEUS (PROfile TElemetry of Upper ocean currentS) moorings were equipped with a 153.6-kHz RD Instruments acoustic Doppler current profiler (ADCP). With this instrument, ocean currents to a depth of 250 m could be measured and data transmitted to shore in real time via Service Argos. However, due to the reflection of acoustic energy from fish in the vicinity of surface moorings, large bias errors were at times found in the ADCP velocities. This report describes the correction of the ADCP velocity errors at 110°W and 140°W from 1993 to 1995 using coincident mechanical current meter (MCM) data. A method is developed that uses empirical orthogonal functions of ADCP-MCM speed differences to correct the ADCP velocities in post processing. Corrected speeds are expected to be accurate to about 5 cm s^{-1} . Beginning in August 1995, the ADCPs at these locations were deployed on subsurface moorings that were free of the fish-bias errors encountered on the surface mooring deployments.

1. Introduction

The Tropical Atmosphere Ocean (TAO) array consists of nearly 70 moorings (Fig. 1) located in the tropical Pacific (Hayes *et al.*, 1991; McPhaden *et al.*, 1998). The purpose of the TAO Array is to measure oceanographic and atmospheric variables in real time in support of El Niño-Southern Oscillation (ENSO) investigations. In addition to ocean temperature and salinity measurements, direct ocean current measurements have been made at the equator where geostrophy does not apply. Early equatorial current measurements were collected with mechanical current meters (MCMs) beginning in 1979 at 110°W , followed later by long-term MCM measurements at 140°W (beginning in 1983) and 165°E (beginning in 1986).

In 1990, the first PROTEUS (PROfile TElemetry of Upper ocean currentS) mooring (McPhaden *et al.*, 1990) was deployed at 0° , 140°W . PROTEUS moorings were equipped with telemetering RD Instruments (RDI) acoustic Doppler current profilers (ADCPs) and transmitted real-time ocean currents within 250 m of the surface (Fig. 2). In 1991 PROTEUS sites were also established at 110°W and 165°E as part of the TAO array. An additional PROTEUS site was established at 0° , 156°E in 1991 as part of the TOGA Coupled Ocean Atmosphere Response (COARE) Experiment (Webster and Lukas, 1992).

However, the accuracy of the surface-mounted ADCP measurements on the PROTEUS moorings was degraded due to the presence of pelagic fish, which were sometimes attracted to the vicinity of the moorings (Freitag *et al.*, 1992; Plimpton *et al.*, 1997). Reflections of the acoustic signal by fish resulted in velocity errors in the ADCP data. In an earlier report by Plimpton *et al.* (1995), a post-processing technique was developed to correct the PROTEUS ADCP data at 0° , 110°W and 0° , 140°W from 1990 to 1993.

In an effort to eliminate fish-bias velocity errors during data acquisition, the authors and RD Instruments (the ADCP manufacturer) developed an

algorithm to reject fish-biased velocities on an individual ping basis before ensemble averaging. All PROTEUS moorings deployed after March 1992 included this algorithm and a decrease in the percentage of good pings per ensemble average occurred during periods when fish were present. This indicated that some rejection of fish-biased data was occurring during data collection, but large velocity errors were still evident. The failure of the ADCP fish-rejection algorithm to eliminate the fish-bias velocity errors resulted in the conversion of the ADCPs to subsurface moorings without the ability for real-time data transmission. The authors determined that subsurface moorings are free of fish bias by evaluation of subsurface equatorial ADCP data at 140°W from the TIWE experiment (Weisberg *et al.*, 1991).

The 110°W and 140°W ADCPs were mounted on surface PROTEUS moorings until August 1995 and September 1995, respectively. This report describes the ADCP fish-bias velocity errors and correction at these sites from 1993 to the end of the surface deployments in 1995. A similar technique to that presented in Plimpton *et al.* (1995) is used to correct the ADCP velocities using the concurrent 1993 to 1995 MCM data. The corrected ADCP profiles retain the high vertical resolution not available from the MCM data. No corrections for fish bias have been made to the PROTEUS ADCP data at 0°, 156°E and 0°, 165°E. These western Pacific sites were relatively free of the fish bias errors detected at 0°, 110°W and 0°, 140°W (Freitag *et al.*, 1993).

2. Instrumentation and Data Processing

PROTEUS moorings were generally recovered and redeployed twice a year (Table 1). The downward-looking 153.6 kHz narrowband ADCPs were set to collect data at a 1-second sample rate for 6 minutes once per hour. The bin width and pulse length were set to 8 m, resulting in a velocity measurement that represented a weighted average over 16 m depth, sampled at 8-m-depth intervals. The ADCP velocities were collected assuming a surface sound speed of 1536 m s⁻¹. Hourly surface sound speeds computed from in situ temperatures measured at the transducer head and historically averaged surface salinities were used to correct the ADCP velocities (Gordon, 1996). Nominal ADCP bin depths, which assume a constant sound speed with depth of 1475.1 cm s⁻¹, were adjusted using an average sound speed profile computed from historical data at a given location. The bin depth correction, which increased with distance from the transducer, was on average 6.2 m at 110°W and 7.3 m at 140°W at a depth of 250 m. The depth error, resulting from use of average rather than contemporaneous sound velocities, was estimated from the standard deviation of the historical sound velocities. At a maximum depth of 250 m, the depth errors were less than 1.7 m at 140°W and 1.3 m at 110°W. The depth-adjusted ADCP data were mapped onto a 5-m depth interval to allow precise comparison of the MCM and ADCP velocities at the MCM depths. The ADCP data at 10 m depth was estimated by linear extrapolation based on vertical gradients between bin 1 at 14 m and bin 2 at 22 m.

Table 1: PROTEUS mooring deployments at 0°, 110°W and 0°, 140°W.

	Latitude	Longitude	Start date	End date
<i>140° W Sites</i>				
PR13	0° 2.1'N	139° 59.1'W	14 Oct 93	26 May 94
PR15	0° 1.8'N	139° 58.2'W	29 May 94	10 Oct 94
PR17	0° 0.8'N	139° 58.7'W	13 Oct 94	20 Mar 95
PR19	0° 0.3'N	139° 56.7'W	23 Mar 95	9 Sep 95
<i>110° W Sites</i>				
PR14	0° 0.7'S	109° 59.0'W	11 Sep 93	4 May 94
PR16	0° 1.2'S	110° 1.2'W	8 Jun 94	17 Sep 94
PR18	0° 0.8'N	110° 1.1'W	20 Sep 94	22 Feb 95
PR20	0° 0.6'N	109° 59.6'W	25 Feb 95	10 Aug 95

Due to the high shear of equatorial velocities, the ADCPs were set to minimize skew error (Pullen *et al.*, 1992). All 1993–1995 PROTEUS mooring ADCPs used a broad bandwidth filter (600 Hz) in the shallower portion of the depth profile where the greatest shear occurs, switching to a narrow bandwidth filter at a depth below the core of the Undercurrent. The ADCPs were equipped with a KVH compass calibrated to an accuracy of $\pm 2.5^\circ$.

The PROTEUS MCMs were either EG&G Vector Averaging Current Meters (VACMs) or Vector Measuring Current Meters (VMCMs). They measured velocities at six or seven specific depths, which could be compared with the ADCP. Small differences occurred in the comparisons due to the ADCP velocity representing a weighted average over 16 m rather than a specific depth. Other small differences were probably caused by MCM measurement errors due to mooring motion. PMEL tow tank tests indicated that VACMs were accurate to within 1.2 cm s^{-1} in steady flow. In highly variable flows, VACMs have been found to overestimate velocity (Beardsley, 1987; Karweit, 1974) and VMCMs have been found to underestimate velocity by a few percent (Weller and Davis, 1980). Halpern (1987) found good agreement in comparisons of VACM/VMCM pairs separated by 1 m on taut-line equatorial moorings. The largest RMS differences were at 13–14 m, equal to 7.4 cm s^{-1} or about 10% of the mean speeds, with smaller differences found at deeper depths. The VMCMs used a flux gate compass, similar to the one used in the ADCP, calibrated to an accuracy of $\pm 2.5^\circ$. During pre-deployment checkout, the VACM mechanical compass linearity (compass error relative to a chosen fixed direction) was confirmed to be $\pm 5.6^\circ$ or less.

Occasionally the MCM at a specific depth would fail before recovery. For the ADCP correction analysis described below, coincident speeds at all six comparison depths were needed. Therefore, the gaps in the MCM coverage, shown in Figs. 3 and 4, had to be filled. Data gaps of 4 days or less were filled by interpolation. In a previous report by Plimpton *et al.*

Table 2: Comparison statistics between existing speeds and speeds computed with multiple linear regression formulae are shown below. Regression fills for MCM data gaps were only used when the correlation coefficient was .89 or greater. Thus, this method for computing missing MCM speeds was not used for 10 m, 120 m, or 200 m at 110°W nor for 80 m at both locations. Statistics are only shown for depths where gaps occurred in the MCM time series.

Depth (m)	Correlation Coefficient	
	110°W	140°W
10	.86	.93
25		.96
45	.90	.90
80	.73	.83
120	.65	
200	.72	

(1995), multiple linear regression (MLR) techniques were used to fill longer gaps in the MCM data at 140°W. To evaluate the feasibility of using this technique to fill missing MCM data at 110°W and 140°W from 1993 to 1995, multiple linear regression formulae were computed based on the time series of speeds at a given depth along with the time series from adjacent depths. Since no data shallower than 10 m nor deeper than 200 m were collected, MLR formulae for the 10-m and 200-m time series were computed based on the 10-m, 25-m, and 45-m time series and the 80-m, 120-m, and 200-m time series, respectively. These formulae were used to compute a time series of speeds at each of the depths where gaps occurred and where data from adjacent depths were available. Statistics derived from a comparison of the computed speeds at 10 m, 25 m, 45 m, 80 m, 120 m, and 200 m with existing speeds at these depths are shown in Table 2. In the earlier report mentioned above (Plimpton *et al.*, 1995), data gaps were filled using MRL formulae when the correlation coefficient between the computed and existing speeds was .89 or greater. The same criteria was used for this study and regression techniques were used to fill 10 m and 25 m data gaps at 140°W and 45 m data gaps at both 110°W and 140°W.

Data gaps at depths of 80 m, 120 m, and 200 m were not filled using MLR techniques due to the low correlation coefficients at these depths. Similarly, the missing 10-m data in the PR16 deployment at 110°W were not filled using MLR techniques. The correlation coefficient for 110°W at 10 m was only .86, significantly lower than the .93 correlation computed for 140°W at 10 m. The lack of correlation at 110°W may be related to the depth of the Equatorial Undercurrent (EUC) at each location. At 140°W, the EUC depth is generally between 75 and 175 m, whereas at 110°W, the EUC depth is about 75 m shallower than at 140°W and often reaches the surface. This increased variability in the 110°W current structure at 10 m, 25 m, and 45 m decreased the correlation of existing speeds with the calculated speeds derived from regression formulae based on these depths.

The MCM data not filled by the MLR technique or interpolation were

filled by careful evaluation of the ADCP data. Information on the evidence of fish bias in the ADCP data is available in the ADCP data from the echo intensity, which is related to the strength of the backscattered acoustic signal for each of the four beams. An increase in echo intensity, which was not related to the diurnal movement of zooplankton, indicated the presence of fish. For deeper depths, 80 m and below, ADCP velocity errors due to the presence of fish appeared to be diurnally modulated as described in Freitag *et al.* (1993). Fish were present during local daylight hours and absent during the night. This allowed a daily average to be computed by averaging the ADCP velocities from the local nighttime hours only (2000 to 0200 local time). These velocities, essentially free of fish bias, were used to fill the MCM data records needed for the EOF analysis described below.

For the PR16 deployment, 10-m MCM data were missing for the period 19 July to 17 September 1994. Since these data could not be filled with the MLR technique, the diurnal presence of fish at 10 m was evaluated for the PR16 deployment. In other deployments, more heavily biased by fish, the depths shallower than 80 m generally had significant fish bias even during local nighttime hours. However, the echo intensities from the PR16 deployment indicated that the ADCP data were essentially free of fish bias for the entire day at all depths through 27 August 1994. For consistency, a daily average was computed from only the nighttime ADCP values to fill the 10-m MCM data gap through 27 August 1994. During the last 21 days of the deployment, the nighttime hours had minimal fish bias at 10 m and an average speed could be computed from 2000 to 0200 local time for all but four of the days. The 10-m speeds for these 4 days were computed by interpolation between the successfully computed nighttime averaged ADCP speeds.

No ADCP or MCM data were collected at 110°W from 5 May thru 7 June 1994.

3. ADCP Velocity Bias

The ADCP transmits an acoustic signal from each of its four beams directed 30 degrees from vertical. The instrument measures the Doppler shift of the return signal for each beam, time gated so as to compute the beam-direction velocity as a function of range. The beam velocities are converted to Earth coordinates using beam geometry and direction from the compass. The frequency shift in the return signal is caused by the relative motion of oceanic scatterers with respect to the ADCP transducers. For the motion of the scatterers to represent ocean velocities, it is assumed that they move passively with the currents. Comparison with the MCM velocities has shown that this assumption fails when pelagic fish are present near the surface moorings. Since the mean movement of these fish is not due to advection by currents, their presence in the ADCP acoustic beam will tend to reduce the magnitude of the velocity measurements. For example, if the scattering intensity of a fish is similar to that of the surrounding water, an individual fish would be detected in one ADCP beam but not the opposing beam. The

horizontal velocity computed from the two beams would be equal to the average of the true ocean current measured in one beam and the current velocity biased by the fish velocity in the second beam. The velocity of fish schooling around a mooring would, in the mean, be small. Thus, when the acoustic reflections from fish are averaged with the reflections from passive scatterers, the ensemble averaged measurement of horizontal velocities would be biased low. Alternately, in the situation where the scattering intensity from a fish is much greater than the surrounding water, the same fish could be detected in the side lobes of the opposing and neighboring beams. The largest side lobe amplitude is down about 35 db from the beam's main lobe and the fish echo intensity in the beam side lobes can be larger than the scattering signal from the surrounding water. In this situation, the horizontal velocity would tend toward zero because the fish-dominated signals in opposing beams would tend to cancel in the computation of horizontal velocity.

The duration and depth range where fish were present around a mooring was quite variable for different deployments. Figures 5 and 6 show the daily ADCP minus MCM speed differences for the deployments at 110°W and 140°W, respectively. The negative sign of the differences represents the decrease in the ADCP speeds due to the presence of fish. At 140°W, the speed differences for the PR13 deployment indicates the presence of fish down to 80 m immediately after the mooring was deployed. In comparison, significant fish bias velocity errors were not evident for the first 2½ months of the PR19 deployment. At 110°W, the fish bias errors appeared less extensive than at 140°W and generally were not evident for several months after the mooring was deployed.

The presence of fish in the acoustic signal was also evaluated using the ADCP echo intensity (EI). Since it was difficult to distinguish whether increased EI was due to diurnal movements of the scatterers or to the presence of fish, the difference in beam-to-beam EI was computed. For a given depth, the highest beam EI was differenced with the lowest beam EI to compute the echo intensity range (EIR). Use of the EIR to determine the presence of fish was most effective when fish were detected in only one to three beams during the averaging period. If fish were detected in all four beams during the averaging period, all beams would have elevated EI's and the EIR magnitudes would be reduced. In Figs. 5 and 6, periods of large EIR are coincident with times of large ADCP speed errors.

4. ADCP Data Correction

The surface moored ADCP time series at 140°W and 110°W is an extensive current velocity data set with high vertical resolution. The velocity errors that occurred at times, due to the presence of fish, had to be corrected before the time series could be included in the TAO data base. A method has been developed to correct the ADCP data in post processing using in situ MCM data by computing empirical orthogonal functions (EOFs) of ADCP-MCM speed differences at the depths of the MCMs.

Mean ADCP and MCM speeds (Figs. 7a–14a) and mean ADCP-MCM

Table 3: Percent variance corrected for each of the first three vertical modes and their total for each deployment.

	Mode 1	Mode 2	Mode 3	Total
<i>110° W Sites</i>				
PR14	71.4	15.0	6.0	92.4
PR16	86.2	5.5	3.5	95.2
PR18	66.3	17.9	11.7	95.9
PR20	71.5	13.8	7.1	92.4
<i>140° W Sites</i>				
PR13	56.0	19.5	17.4	92.9
PR15	71.9	17.0	6.1	95.0
PR17	56.4	28.0	6.3	90.7
PR19	77.9	10.4	4.9	93.2

speed differences (Figs. 7b–14b) were computed for each deployment. A spline fit was performed on the speed differences at the MCM depths to create values at all intervening ADCP depths. For each deployment, the spline fit was forced to 0 at 200 m. This was because fish bias was generally negligible from 200 to 250 m, which was evident from the minimal values for ADCP-MCM speed differences and EIR at these depths (Figs. 5 and 6). The small differences that were evident may have been from instrument measurement differences or overspeeding by the VACMs (Halpern, 1987).

For each deployment, the mean speed differences were subtracted from the ADCP-MCM time series before computing the EOFs. A spline fit, forced to 0 at 200 m, was performed on the eigenvectors for each eigenmode to create values at the ADCP depths. The first three eigenmodes for each deployment are shown in Figs. 15 to 22.

Only the first three eigenmodes were used in this correction scheme because the difference between the ADCP and the MCM speeds were not all due to the presence of fish. Higher EOF modes may have captured more subtle forms of instrument error in the MCMs and/or the ADCPs. Likewise, some of the ADCP-MCM differences were probably due to the fact that the ADCP velocity represents a weighted mean over 16 m compared to the MCM velocity, which applies to a specific depth. Table 3 lists the percent variance corrected for each of the first three vertical modes for each deployment. For all deployments, more than 90% of the variance was explained by these three modes.

For each deployment, the means and first three vertical modes were combined to produce a correction file for the daily ADCP speeds at the ADCP depths. When the corrected ADCP speeds were compared with the MCM speeds, there was considerable reduction in the standard deviation of the speed differences for each deployment (Figs. 7c to 14c). Comparison of the MCM and the ADCP daily directions indicated that errors in the ADCP directions occurred due to the presence of fish. The direction errors were

evident when measured ADCP speeds less than 10 cm s^{-1} were increased by more than 50 cm s^{-1} during correction by the EOF analysis. At these times, the daily averaged ADCP directions would have included measurements where the fish-biased speeds were often near zero value and the directions were meaningless. At other times, when the daily ADCP speed bias was smaller, the ADCP directions did not appear affected by the presence of fish. Thus, daily profiles of zonal and meridional velocity were first computed using all the ADCP directions and the corrected ADCP speeds. Then the ADCP data were flagged bad when measured speeds of 10 cm s^{-1} or less increased by at least 50 cm s^{-1} after correction and, for the MCM depths, when corrected ADCP-MCM zonal or meridional velocity differences were greater than 10 cm s^{-1} . These data were identified on a bin by bin basis for each daily profile and deleted from the ADCP data base. ADCP directions for earlier 1990 to 1993 PROTEUS deployments, which were previously documented in Plimpton *et al.* (1995) and included in the TAO archive, were also reexamined and edited using these procedures.

After the fish-biased ADCP directions were eliminated from the data set, the ADCP and MCM directions were again compared. The mean ADCP-MCM direction differences (Figs. 7d–14d) were used to identify compass errors that may not have been detected in the routine evaluation of the current meter data. The ADCP directions for the PR17 deployment were rotated by -5° . The PR17 ADCP compass error was evident in the large mean ADCP-MCM direction differences at all the MCM depths and the apparently large meridional velocity at the depth of the Undercurrent. MCM directions were corrected when the mean difference between the edited ADCP daily directions and the MCM directions at a given depth exceeded 10° . The MCM directions were then adjusted so that the mean ADCP-MCM difference was equal to the average differences found at the other depths for the deployment. The final adjusted directions were used in Figs. 7–14.

The corrected and edited zonal and meridional velocities for the eight deployments described above were included in the TAO ADCP data base. Contour plots of these velocities from 1993–1995 at 110°W and 140°W are shown in Figs. 23 and 24, respectively.

5. Summary

Beginning in 1990, PROTEUS mooring sites were established as part of the TAO array to measure and transmit real-time currents in the upper ocean with an ADCP. However, PROTEUS velocity measurements were at times biased toward lower values due to the reflections from pelagic fish in the acoustic beams of ADCPs mounted on surface moorings. As a result of the velocity errors, an algorithm was developed to try to remove fish-bias errors during data acquisition. Although some fish-biased data were rejected by the algorithm during data collection, the algorithm essentially failed and large errors were still evident in the ADCP velocities. For these reasons, the use of PROTEUS moorings in TAO was stopped in 1995, and all subsequent

equatorial ADCPs were mounted on subsurface moorings. The subsurface ADCP data were free of the fish bias found in surface deployments.

The extent of the fish-bias errors in the 1990 to 1995 surface moored ADCP data were evaluated by computing the ADCP echo intensity range and by comparison with in situ MCM data. The error description and correction for the 1990 to 1993 ADCP data at 110°W and 140°W are presented in Plimpton *et al.* (1995). The 1993 to 1995 ADCP velocity errors at 110°W and 140°W are described above. A procedure based on an EOF analysis of ADCP-MCM speed differences, similar to that used for the earlier data, were used to correct the ADCP velocities for this period. The corrected speeds are expected to be accurate to about 5 cm s⁻¹. This estimate was derived from comparison of two coincident ADCP deployments at 140° in 1993 (Plimpton *et al.*, 1995; Plimpton *et al.*, 1997). The corrected ADCP profiles of daily zonal and meridional velocities have been included in the TAO data base. These data provide velocities with a finer vertical resolution and fewer data gaps than previously available with the MCM data.

6. Acknowledgments

This work was supported by NOAA's office of Global Programs and NOAA's Environmental Research Laboratories.

7. References

- Beardsley, R.C. (1987): A comparison of the vector-averaging current meter and New Edgerton, Germeshausen, and Grier, Inc., vector-measuring current meter on a surface mooring in Coastal Dynamics Experiment 1. *J. Geophys. Res.*, *92*, 1845–1859.
- Freitag, H.P., M.J. McPhaden, and P.E. Pullen (1992): Fish-induced bias in acoustic Doppler current profiler data. *Proceedings of Oceans '92, Mastering the Oceans Through Technology*, 26–29 October 1992, Newport, RI, 712–717.
- Freitag, H.P., P.E. Plimpton, and M.J. McPhaden (1993): Evaluation of an ADCP fish-bias rejection algorithm. *Proceedings of Oceans '93, Engineering in Harmony with the Ocean*, Vol. II, 18–21 October 1993, Victoria, Canada, 394–397.
- Gordon, R.L. (1996): Acoustic Doppler current profilers, principles of operation: A practical primer. R.D. Instruments, 51 pp. (Available from R.D. Instruments, 9855 Businesspark Ave., San Diego, CA 92131.)
- Halpern, D. (1987): Comparison of upper ocean VACM and VMCM observations in the equatorial Pacific. *J. Atmos. Ocean. Tech.*, *4*, 84–93.
- Hayes, S.P., L.J. Mangum, J. Picaut, A. Sumi, and K. Takeuchi (1991): TOGA-TAO: A moored array for real-time measurements in the tropical Pacific Ocean. *Bull. Am. Meteorol. Soc.*, *72*, 339–347.
- Karweit, M. (1974): Response of a Savonius rotor to unsteady flow. *J. Mar. Res.*, *32*, 359–364.
- McPhaden, M.J., H.B. Milburn, A.I. Nakamura, and A.J. Shepherd (1990): PROTEUS—Profile telemetry of upper ocean currents. *Proceedings of the MTS '90 Conference*, Washington, DC, 26–28 September, Marine Technology Society, Washington, DC, 353–357.
- McPhaden, M.J., A.J. Busalacchi, R. Cheney, J.R. Donguy, K.S. Gage, D. Halpern, M. Ji, P. Julian, G. Meyers, G.T. Mitchum, P.P. Niiler, J. Picaut, R.W.

- Reynolds, N. Smith, and K. Takeuchi (1998): The Tropical Ocean Global Atmosphere observing system: A decade of progress. *J. Geophys. Res.*, *103*(C7), 14,169–14,240.
- Plimpton, P.E., H.P. Freitag, and M.J. McPhaden (1995): Correcting moored ADCP data for fish-bias errors at 0° , 110°W and 0° , 140°W from 1990 to 1993. NOAA Tech. Memo. ERL PMEL-107 (NTIS PB95-219366), 49 pp.
- Plimpton, P.E., H.P. Freitag, and M.J. McPhaden (1997): ADCP velocity errors from pelagic fish schooling around equatorial moorings. *J. Atmos. Ocean. Tech.*, *14*, 1212–1223.
- Pullen, P.E., M.J. McPhaden, H.P. Freitag, and J. Gast (1992): Surface wave induced skew errors in acoustic Doppler current profiler measurements from high shear regimes. *Proceedings of Oceans '92, Mastering the Oceans Through Technology*, 26–29 October 1992, Newport, RI, 706–711.
- Webster, P.J., and R. Lukas (1992): TOGA-COARE: The Coupled Ocean-Atmosphere Response Experiment. *Bull. Amer. Meteorol. Soc.*, *73*, 1377–1416.
- Weisberg, R.H., J.C. Donovan, and R.D. Core (1991): The tropical instability wave experiment (TIWE) equatorial array. University of South Florida Data Report, St. Petersburg, FL, 84 pp.
- Weller, R.A., and R.E. Davis (1980): A vector-measuring current meter. *Deep-Sea Res.*, *27*, 575–582.

Figures

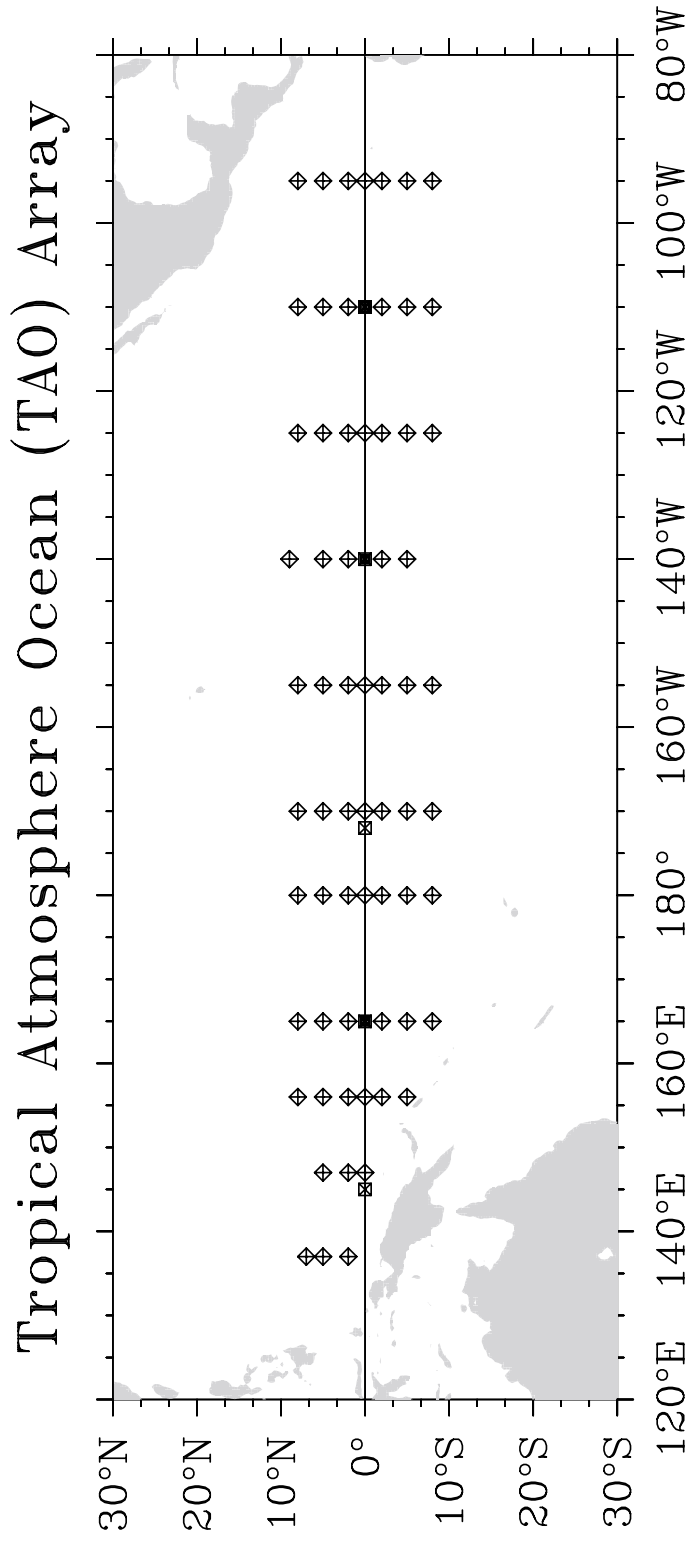


Figure 1: Tropical Atmosphere Ocean (TAO) array of ATLAS moorings (diamonds) and current meter moorings (squares). Solid squares indicate sites instrumented with telemetering PROTEUS current meter moorings prior to 1995. At 110°W, 140°W, and 165°E, the ADCPs previously on surface moorings are now deployed on subsurface moorings.

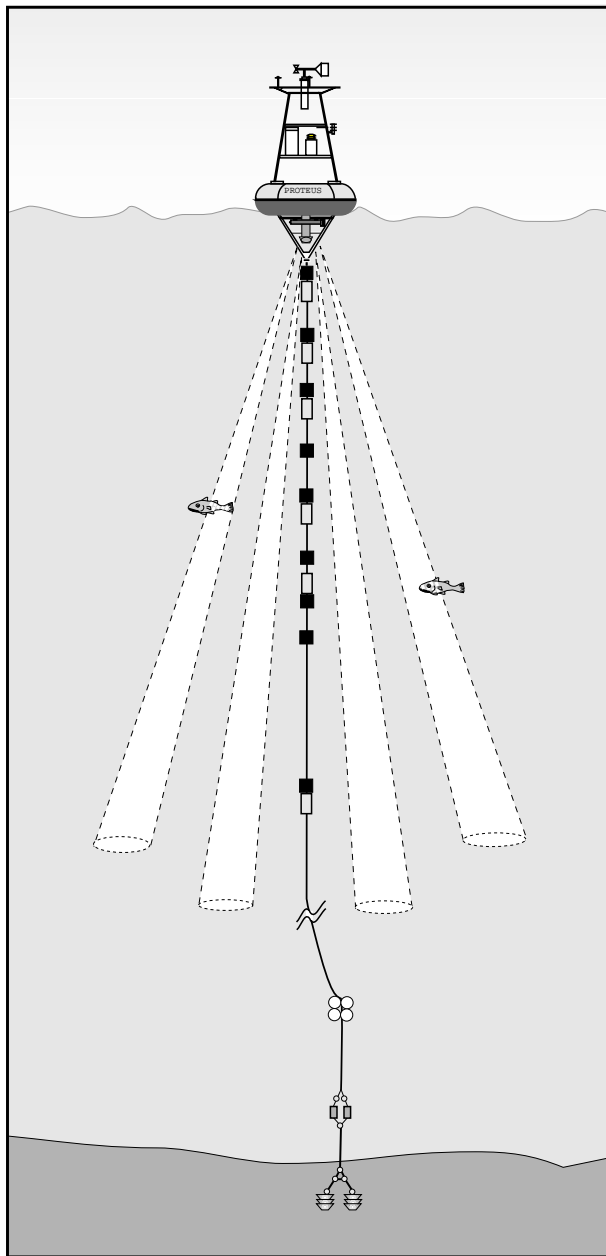


Figure 2: PROTEUS mooring with atmospheric sensors, an ADCP, mechanical current meters (open squares), and temperature sensors (solid squares).

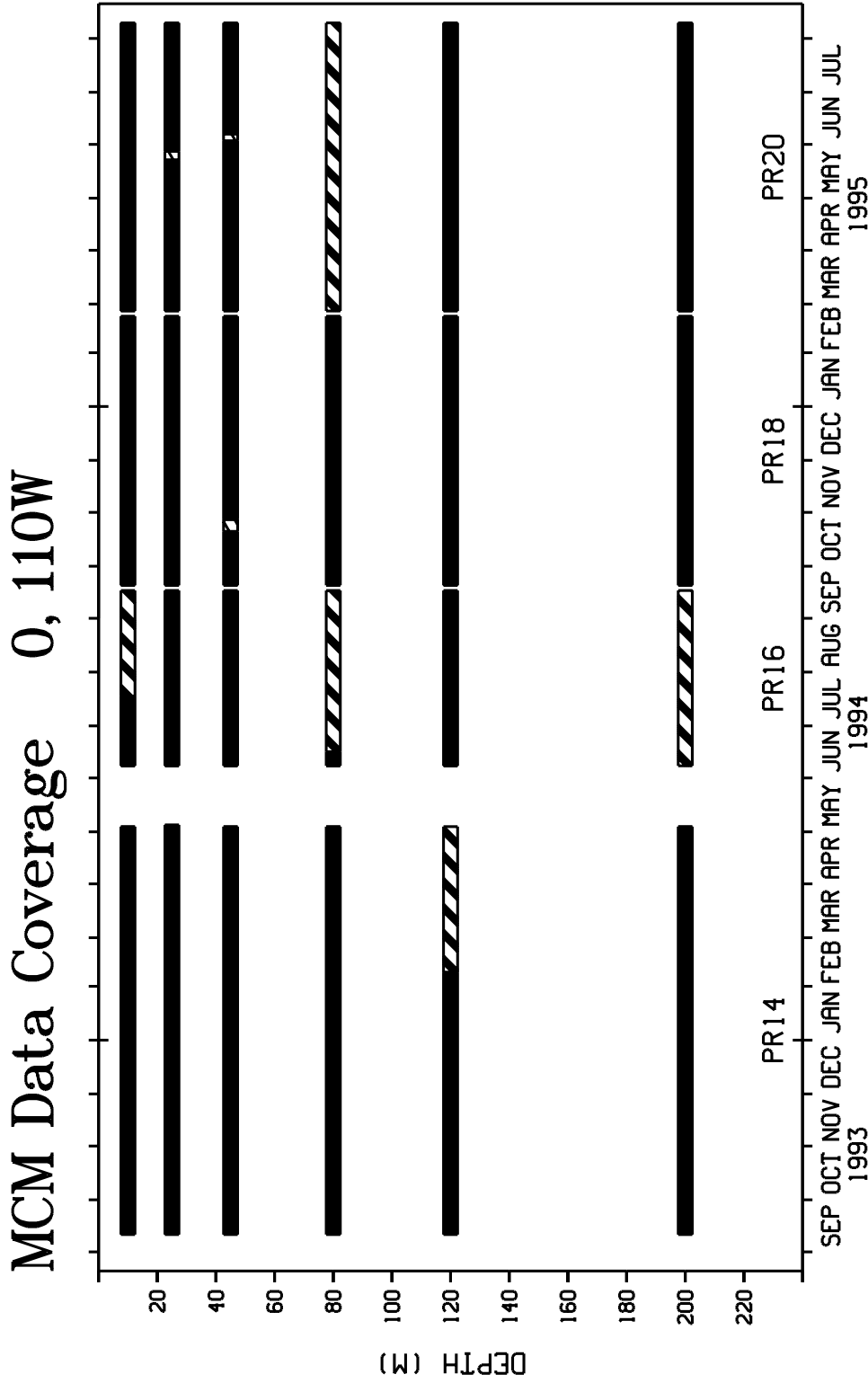


Figure 3: Depth and time coverage of mechanical current meter data at 0°, 110°W. Areas of thin striping at 25 m and 45 m are data filled using interpolation or linear regression techniques. Thick striping at 10 m, 80 m, 120 m, and 200 m indicate gaps filled using ADCP data from the portion of the day that was minimally affected by fish. Due to problems with the MCM compass, only speed data are available at 200 m for the entire PR14 deployment and from December 2 to February 22 for the PR18 deployment.

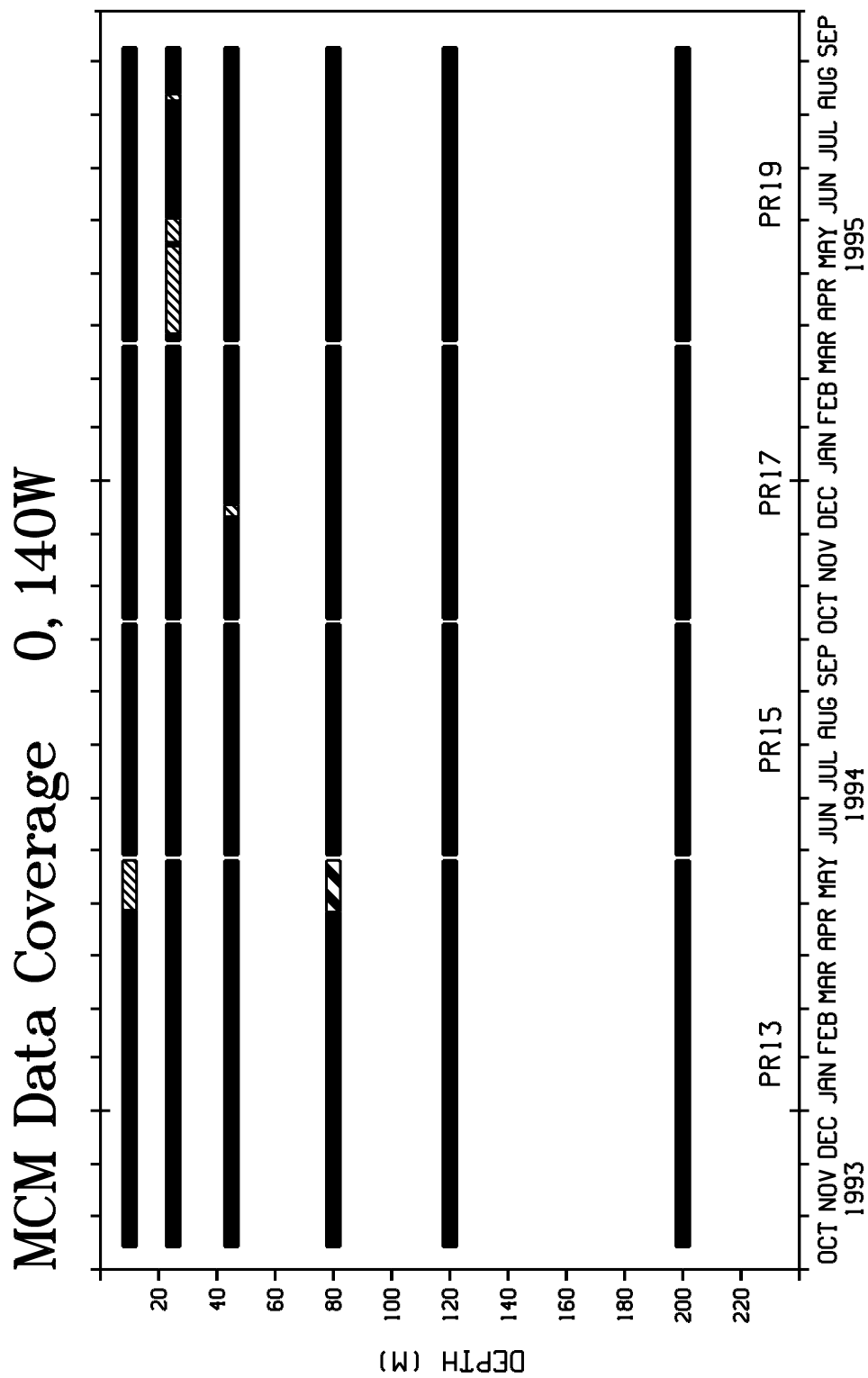


Figure 4: Depth and time coverage of mechanical current meter data at 0° , 140° W. Areas of thin striping at 10 m, 25 m, and 45 m are data filled using interpolation or linear regression techniques. The thick striping at 80 m indicates a data gap filled using ADCP data from the portion of the day that was minimally affected by fish. Due to MCM compass problems, only speed data are available at 80 m from April 11 to September 9 for the PR19 deployment.

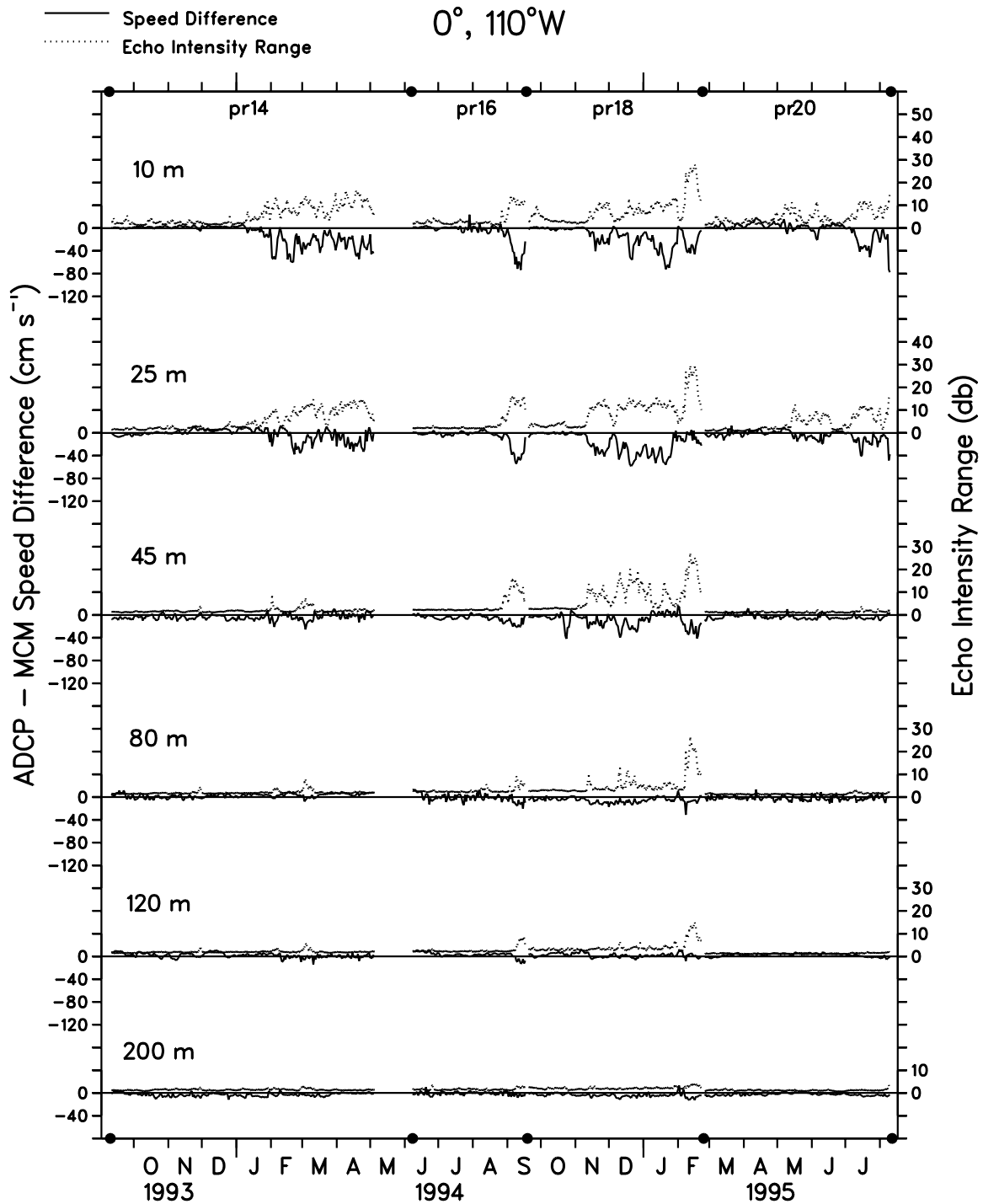


Figure 5: Time series of ADCP-MCM speed difference and echo intensity range for four deployments at 0°, 110°W. Deployment and recovery times of the moorings are shown by black dots at the abscissas. At 10 m depth, the ADCP speed data have been linearly extrapolated from the bin 1 depth of 14 m for the comparison.

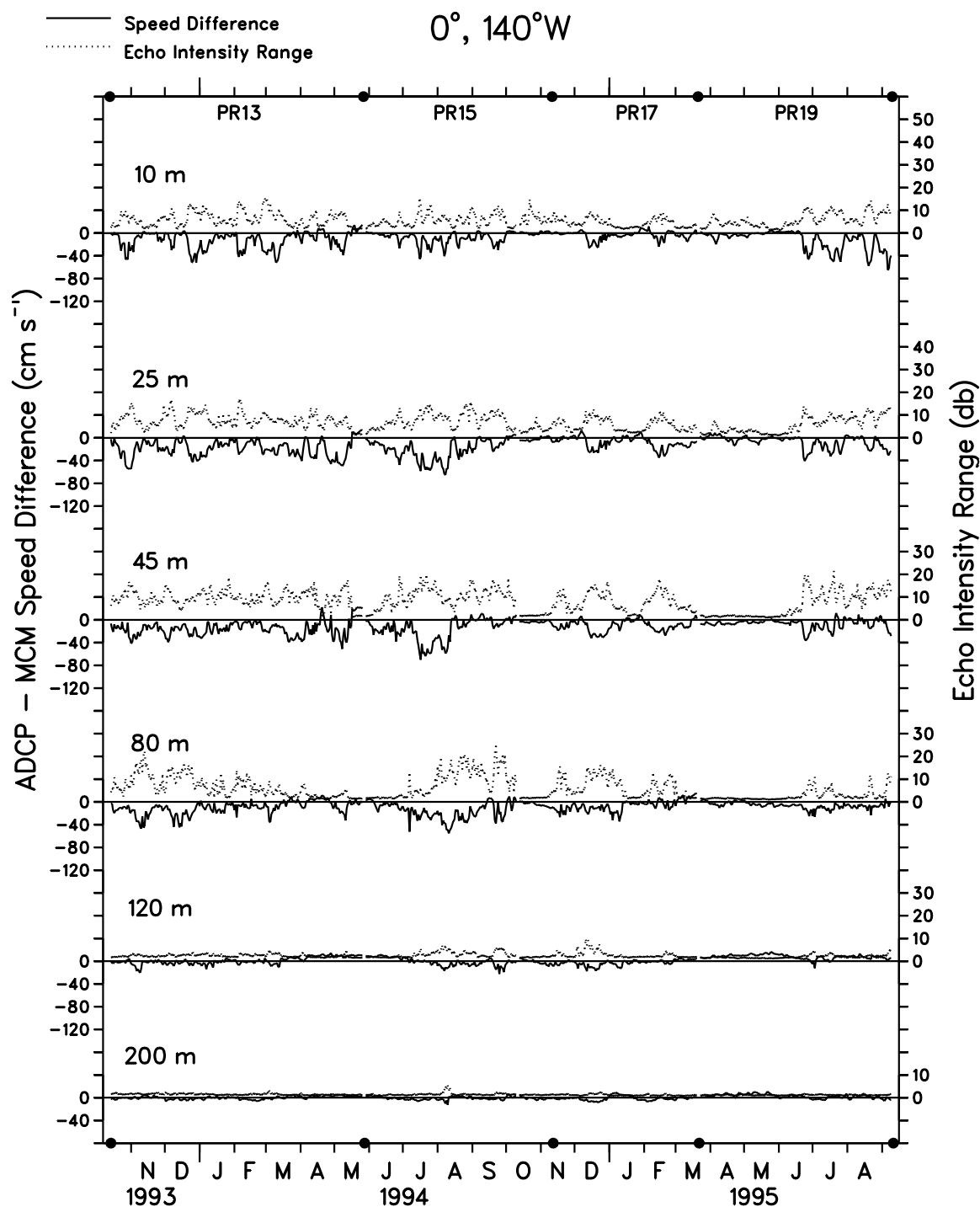


Figure 6: Time series of ADCP-MCM speed difference and echo intensity range for four deployments at $0^\circ, 140^\circ\text{W}$. Deployment and recovery times of the moorings are shown by black dots at the abscissas. At 10 m depth, the ADCP speed data have been linearly extrapolated from the bin 1 depth of 14 m for the comparison.

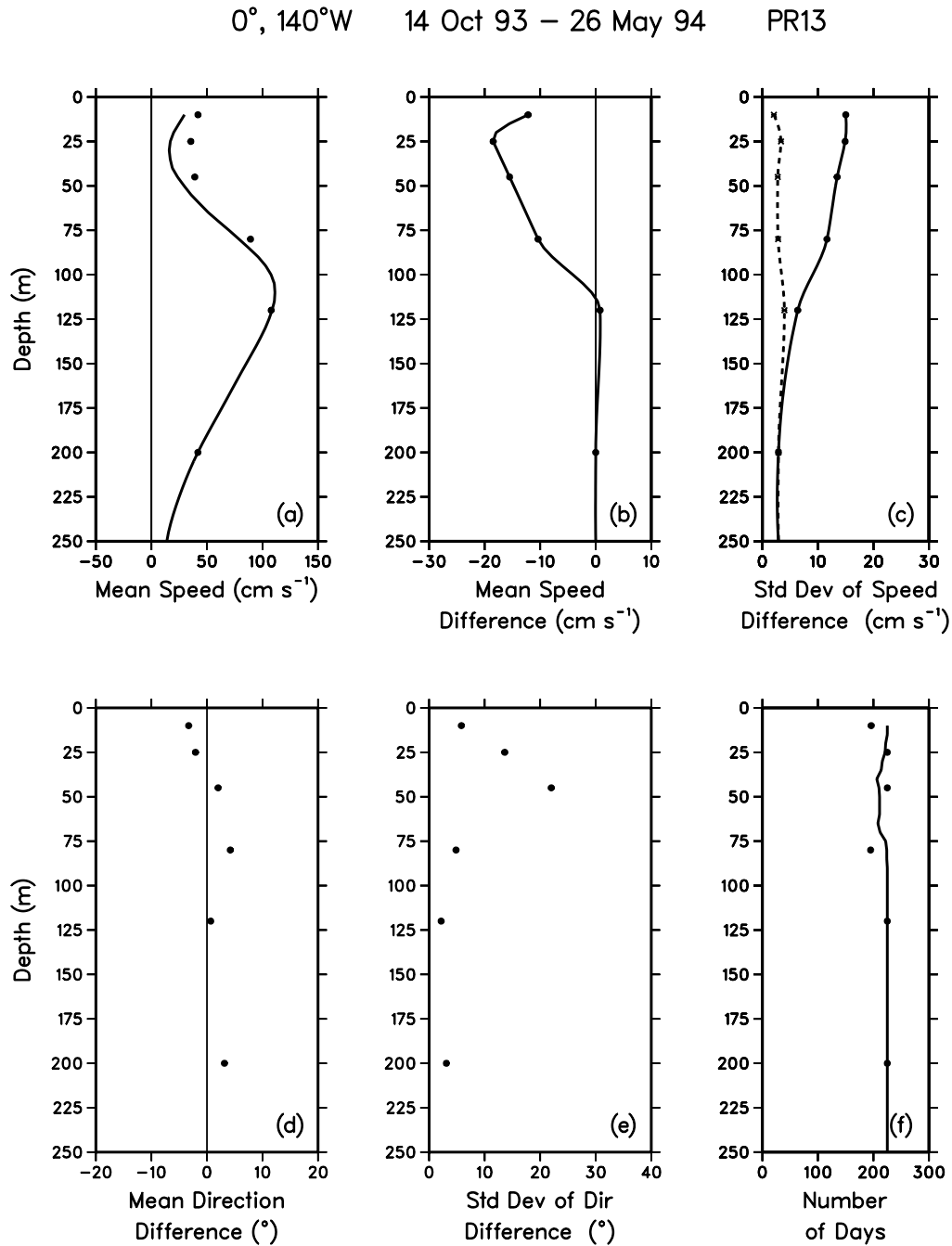


Figure 7: Profiles of (a) mean speed for MCM data (circles) and ADCP data (solid curve), (b) mean ADCP-MCM speed difference (circles) and spline fit to the difference (solid curve), (c) standard deviation of speed difference before EOF correction (solid curve) and after correction (dashed curve), (d) mean ADCP-MCM direction difference, (e) standard deviation of direction difference, and (f) number of days of data collected for MCM (circles) and number of days of ADCP data after correction and editing (solid curve).

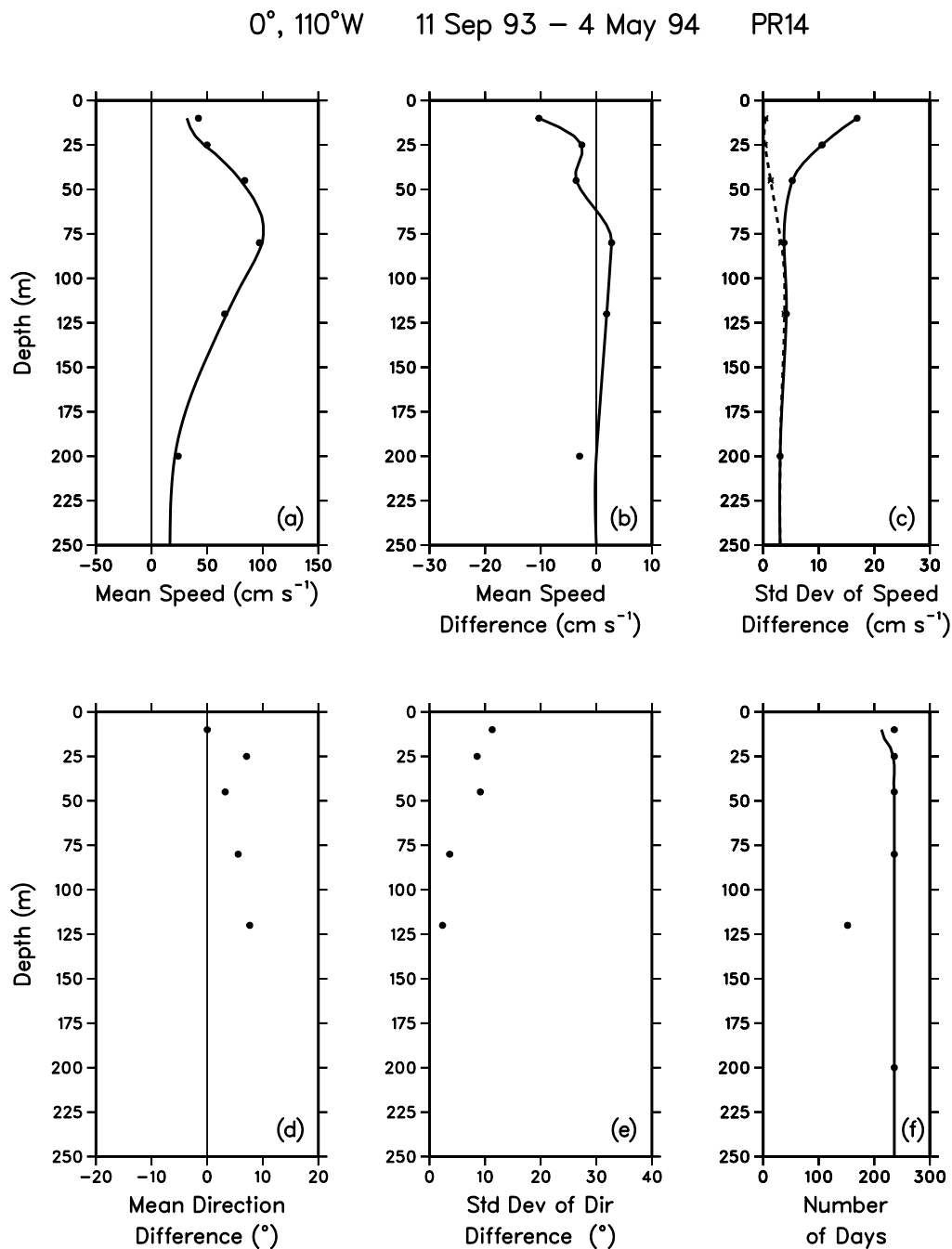


Figure 8: Profiles of (a) mean speed for MCM data (circles) and ADCP data (solid curve), (b) mean ADCP-MCM speed difference (circles) and spline fit to the difference (solid curve), (c) standard deviation of speed difference before EOF correction (solid curve) and after correction (dashed curve), (d) mean ADCP-MCM direction difference, (e) standard deviation of direction difference, and (f) number of days of data collected for MCM (circles) and number of days of ADCP data after correction and editing (solid curve). Due to MCM compass problems, only MCM speeds were available at 200 m for the entire deployment period.

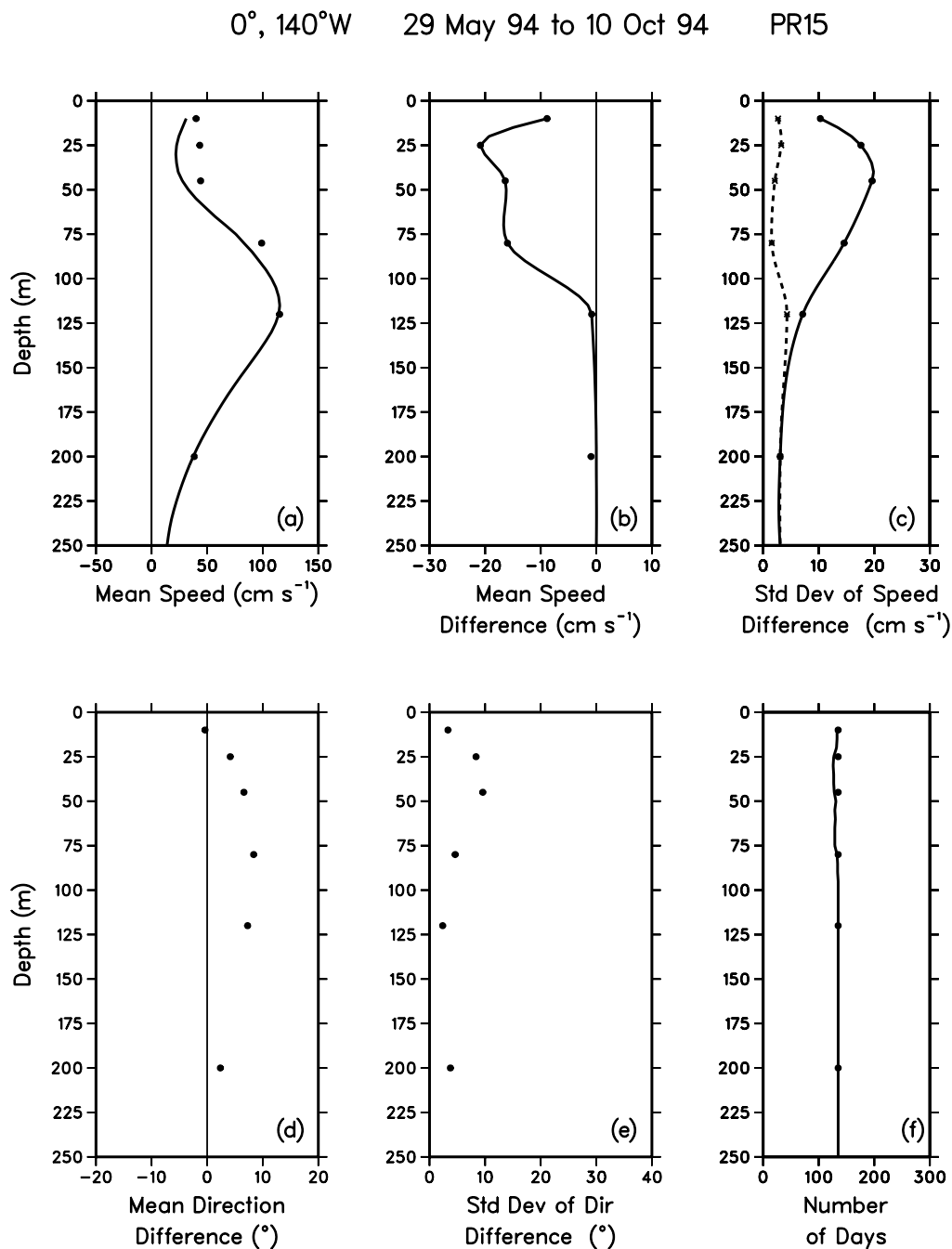


Figure 9: Profiles of (a) mean speed for MCM data (circles) and ADCP data (solid curve), (b) mean ADCP-MCM speed difference (circles) and spline fit to the difference (solid curve), (c) standard deviation of speed difference before EOF correction (solid curve) and after correction (dashed curve), (d) mean ADCP-MCM direction difference, (e) standard deviation of direction difference, and (f) number of days of data collected for MCM (circles) and number of days of ADCP data after correction and editing (solid curve).

0°, 110°W 8 Jun 94 to 17 Sep 94 PR16

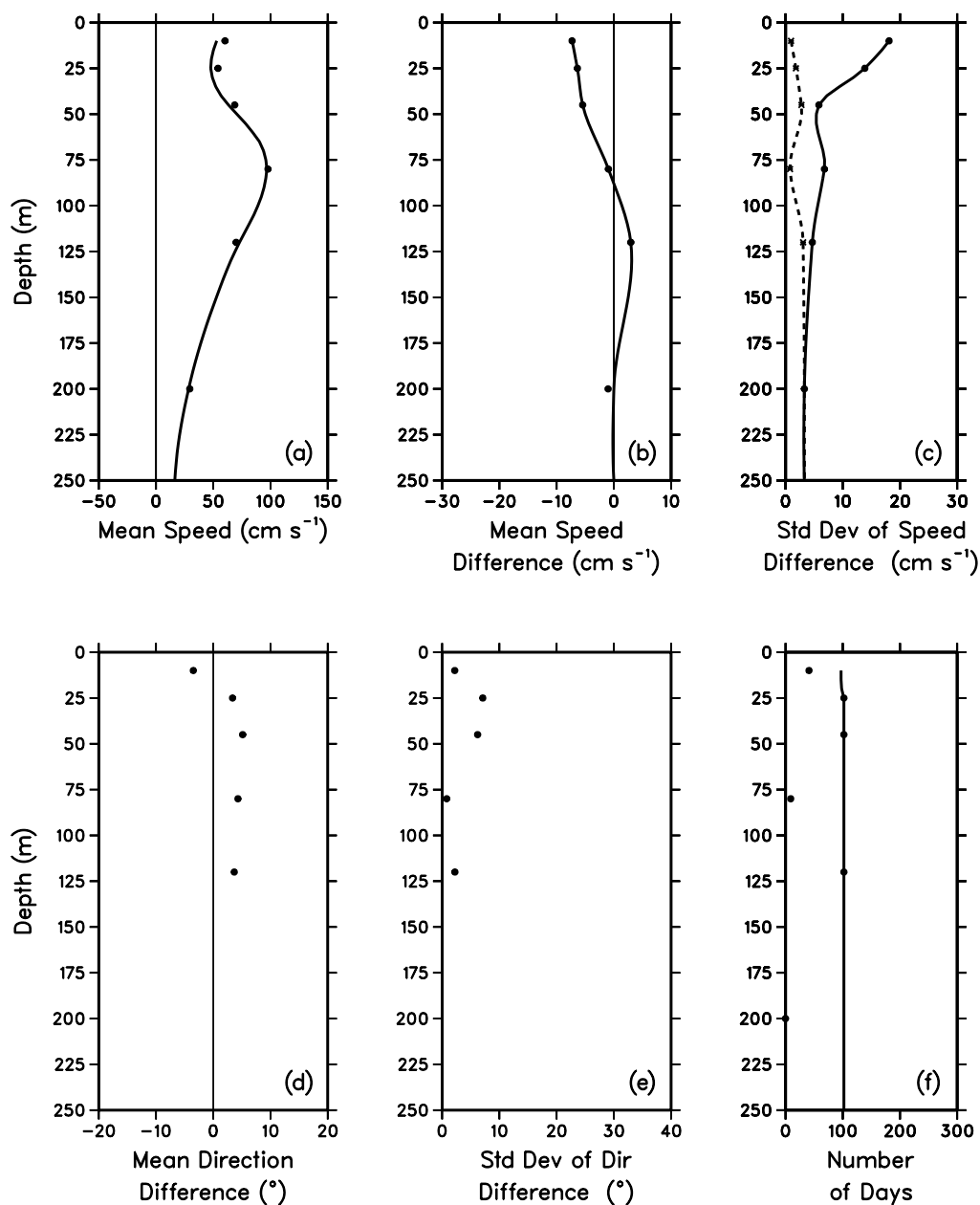


Figure 10: Profiles of (a) mean speed for MCM data (circles) and ADCP data (solid curve), (b) mean ADCP-MCM speed difference (circles) and spline fit to the difference (solid curve), (c) standard deviation of speed difference before EOF correction (solid curve) and after correction (dashed curve), (d) mean ADCP-MCM direction difference, (e) standard deviation of direction difference, and (f) number of days of data collected for MCM (circles) and number of days of ADCP data after correction and editing (solid curve).

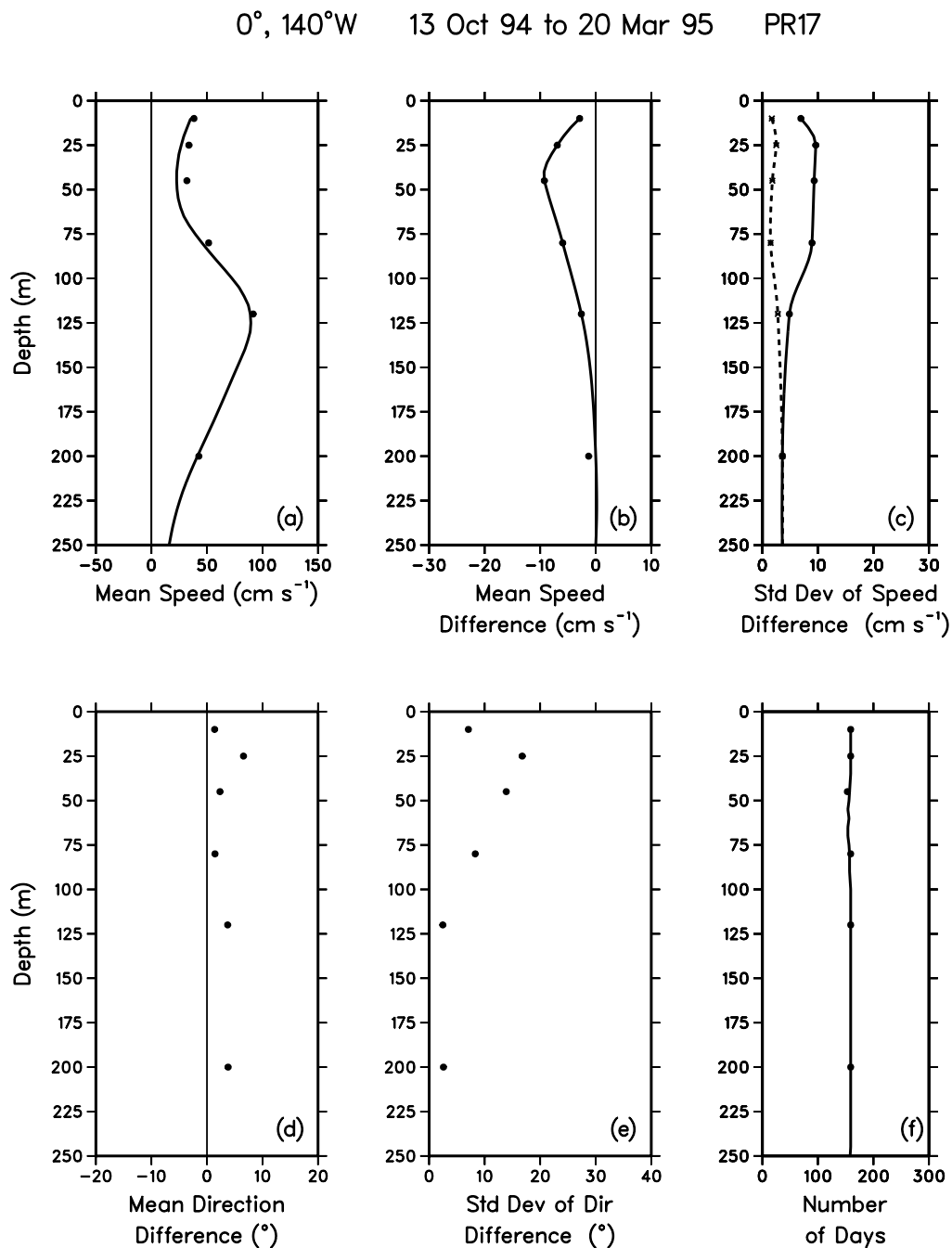


Figure 11: Profiles of (a) mean speed for MCM data (circles) and ADCP data (solid curve), (b) mean ADCP-MCM speed difference (circles) and spline fit to the difference (solid curve), (c) standard deviation of speed difference before EOF correction (solid curve) and after correction (dashed curve), (d) mean ADCP-MCM direction difference, (e) standard deviation of direction difference, and (f) number of days of data collected for MCM (circles) and number of days of ADCP data after correction and editing (solid curve).

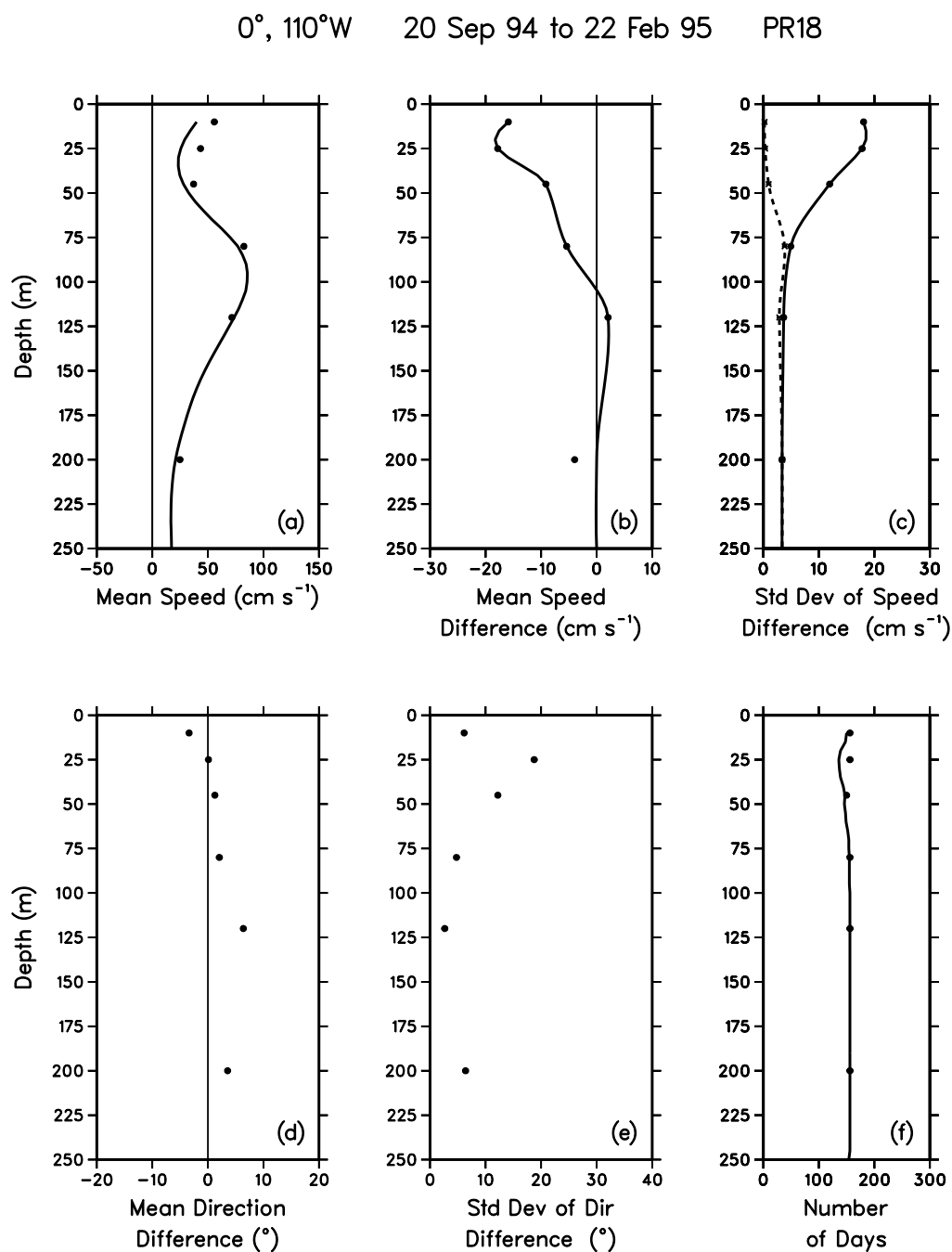


Figure 12: Profiles of (a) mean speed for MCM data (circles) and ADCP data (solid curve), (b) mean ADCP-MCM speed difference (circles) and spline fit to the difference (solid curve), (c) standard deviation of speed difference before EOF correction (solid curve) and after correction (dashed curve), (d) mean ADCP-MCM direction difference, (e) standard deviation of direction difference, and (f) number of days of data collected for MCM (circles) and number of days of ADCP data after correction and editing (solid curve). Due to MCM compass problems, only MCM speeds were available at 200 m from December 2–February 22.

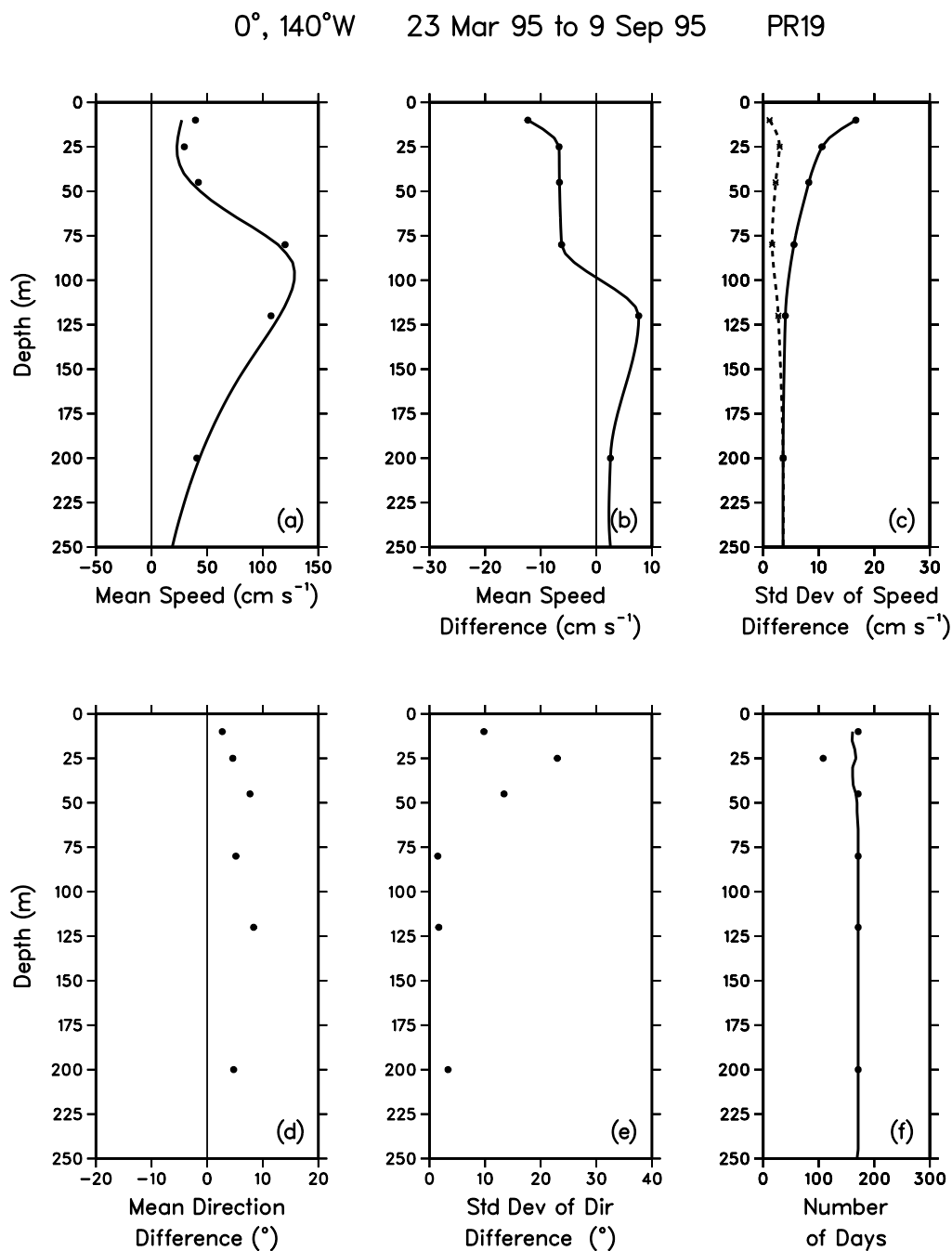


Figure 13: Profiles of (a) mean speed for MCM data (circles) and ADCP data (solid curve), (b) mean ADCP-MCM speed difference (circles) and spline fit to the difference (solid curve), (c) standard deviation of speed difference before EOF correction (solid curve) and after correction (dashed curve), (d) mean ADCP-MCM direction difference, (e) standard deviation of direction difference, and (f) number of days of data collected for MCM (circles) and number of days of ADCP data after correction and editing (solid curve). Due to MCM compass problems, only MCM speeds were available at 80 m from April 11 to September 9.

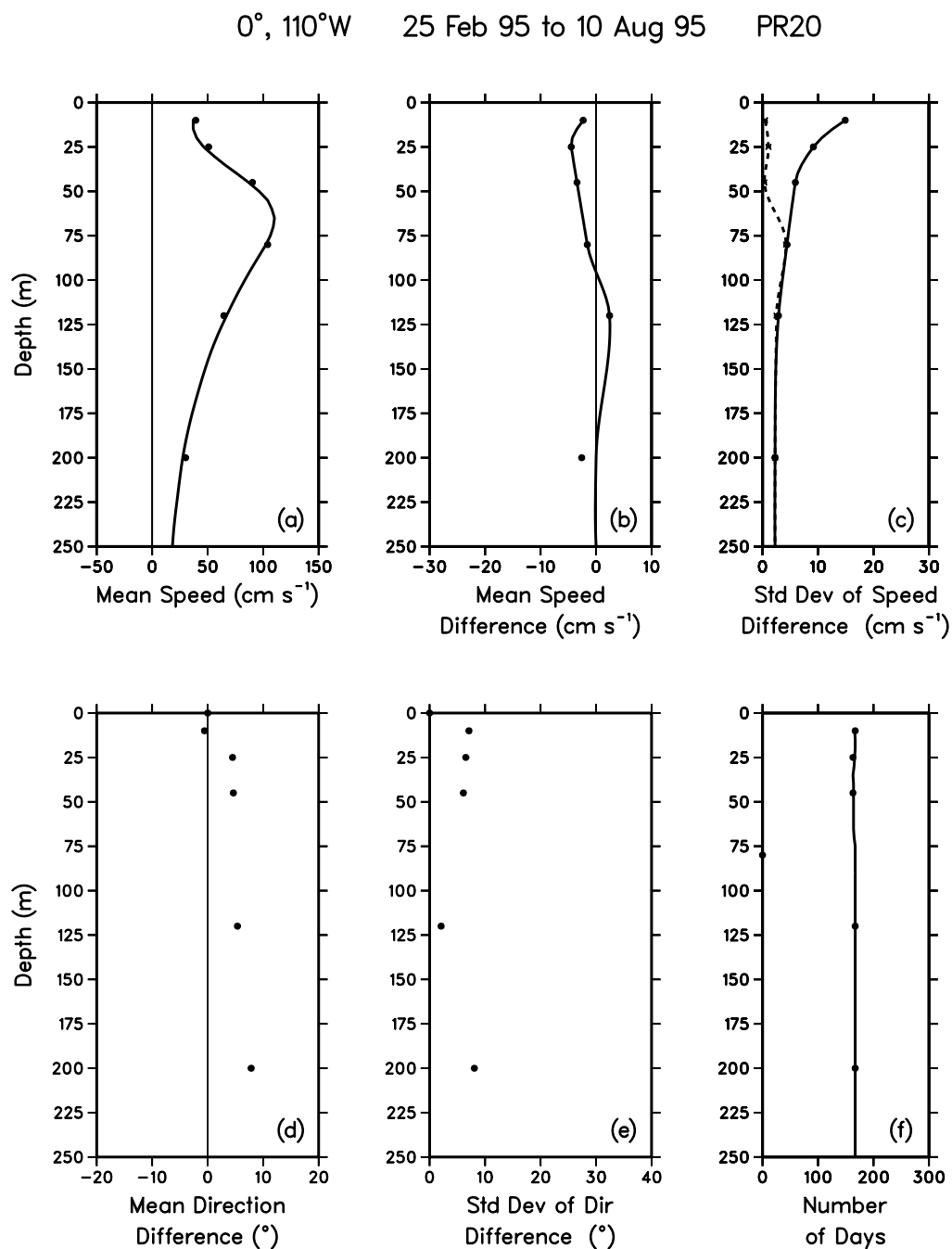


Figure 14: Profiles of (a) mean speed for MCM data (circles) and ADCP data (solid curve), (b) mean ADCP-MCM speed difference (circles) and spline fit to the difference (solid curve), (c) standard deviation of speed difference before EOF correction (solid curve) and after correction (dashed curve), (d) mean ADCP-MCM direction difference, (e) standard deviation of direction difference, and (f) number of days of data collected for MCM (circles) and number of days of ADCP data after correction and editing (solid curve).

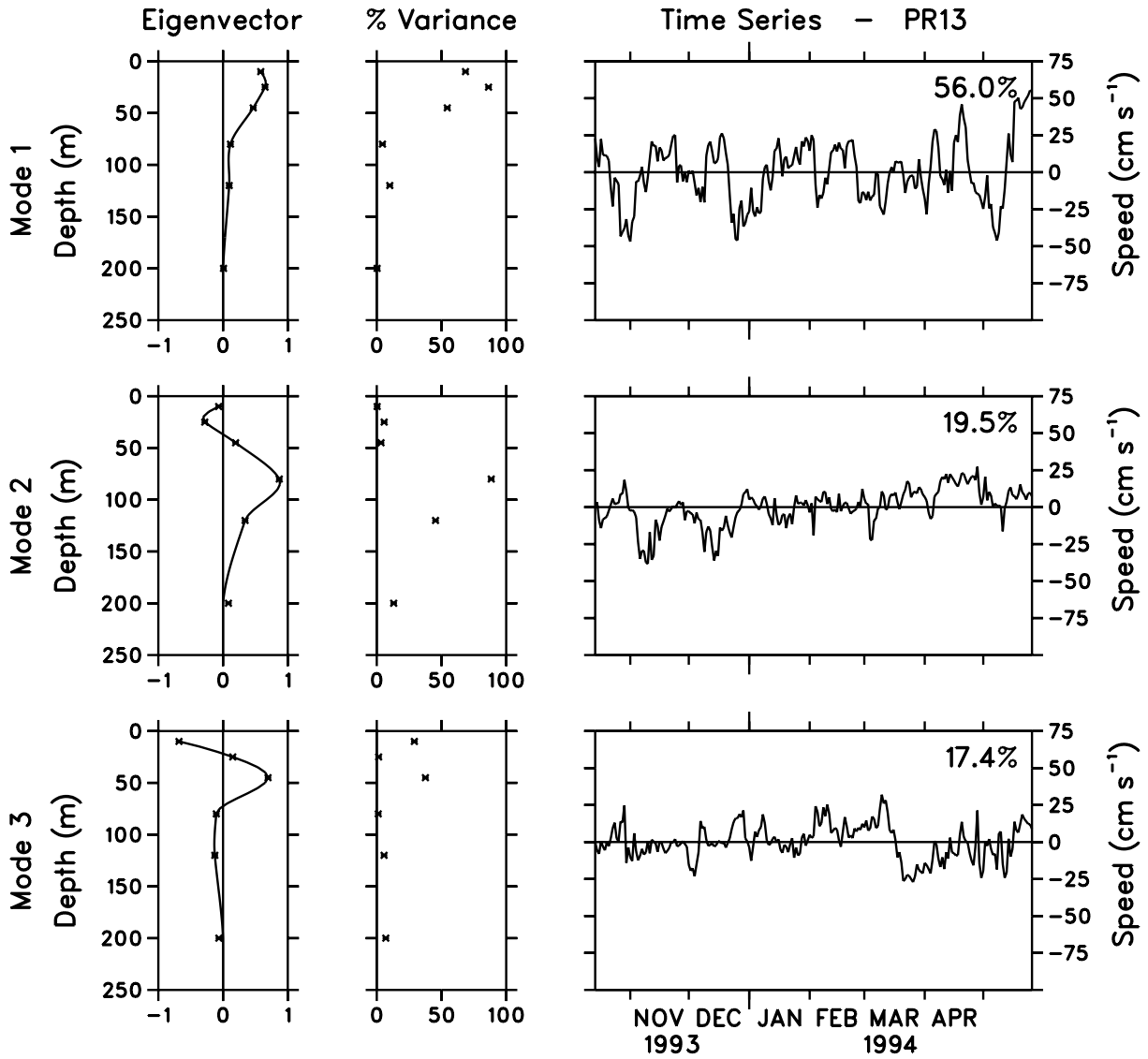


Figure 15: The first three EOF eigenvectors and time series of ADCP-MCM speed differences for PR13. Percent variance explained at each depth is shown in the center panel. Percent of total variance explained by each EOF is shown in the upper right hand corner of the time series panel. The symbols (\times) indicate values at individual MCM depths; the solid curve through the individual eigenvector values is a spline fit which has been forced to zero at 200 m.

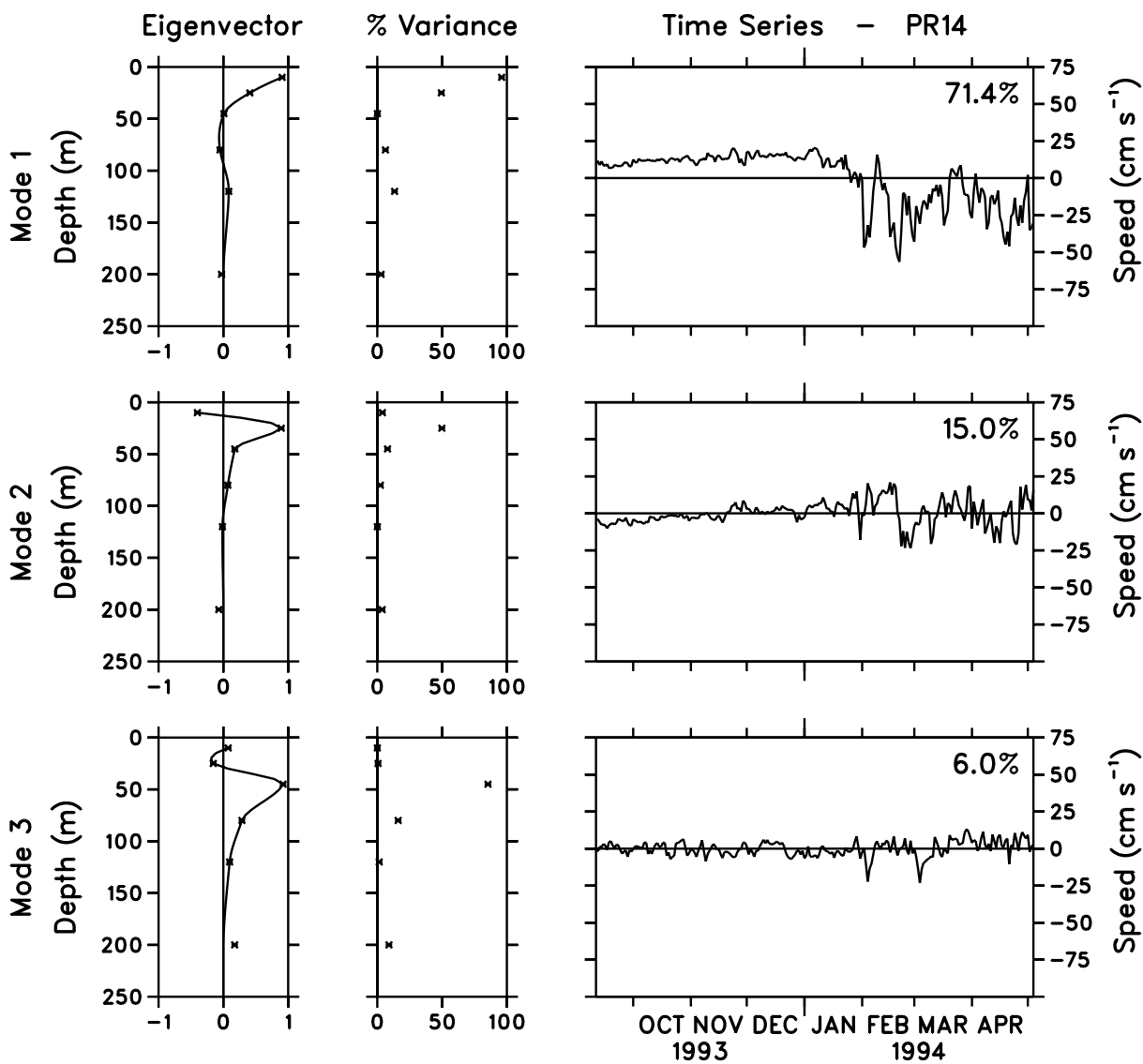


Figure 16: The first three EOF eigenvectors and time series of ADCP-MCM speed differences for PR14. Percent variance explained at each depth is shown in the center panel. Percent of total variance explained by each EOF is shown in the upper right hand corner of the time series panel. The symbols (x) indicate values at individual MCM depths; the solid curve through the individual eigenvector values is a spline fit which has been forced to zero at 200 m.

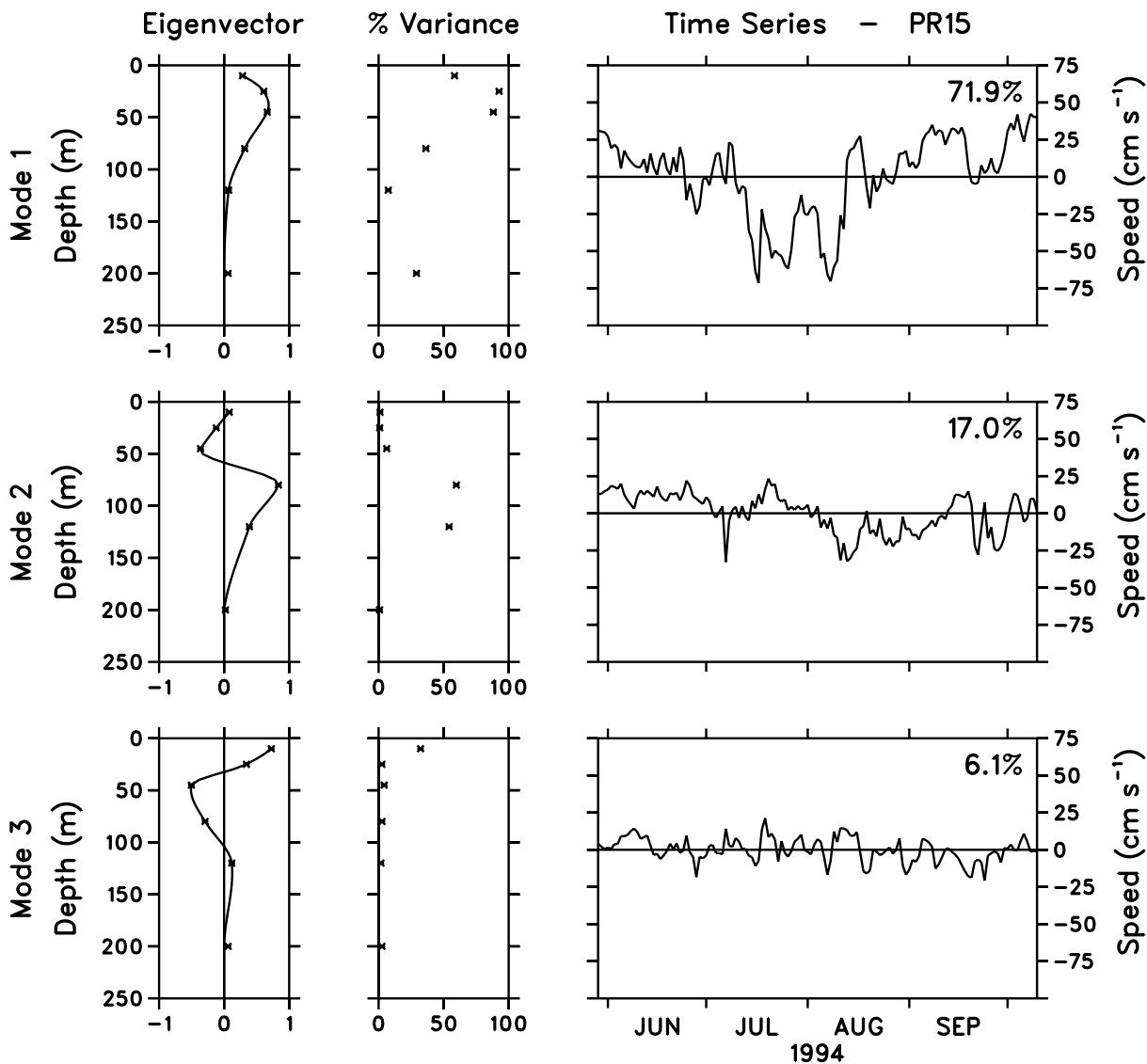


Figure 17: The first three EOF eigenvectors and time series of ADCP-MCM speed differences for PR15. Percent variance explained at each depth is shown in the center panel. Percent of total variance explained by each EOF is shown in the upper right hand corner of the time series panel. The symbols (\times) indicate values at individual MCM depths; the solid curve through the individual eigenvector values is a spline fit which has been forced to zero at 200 m.

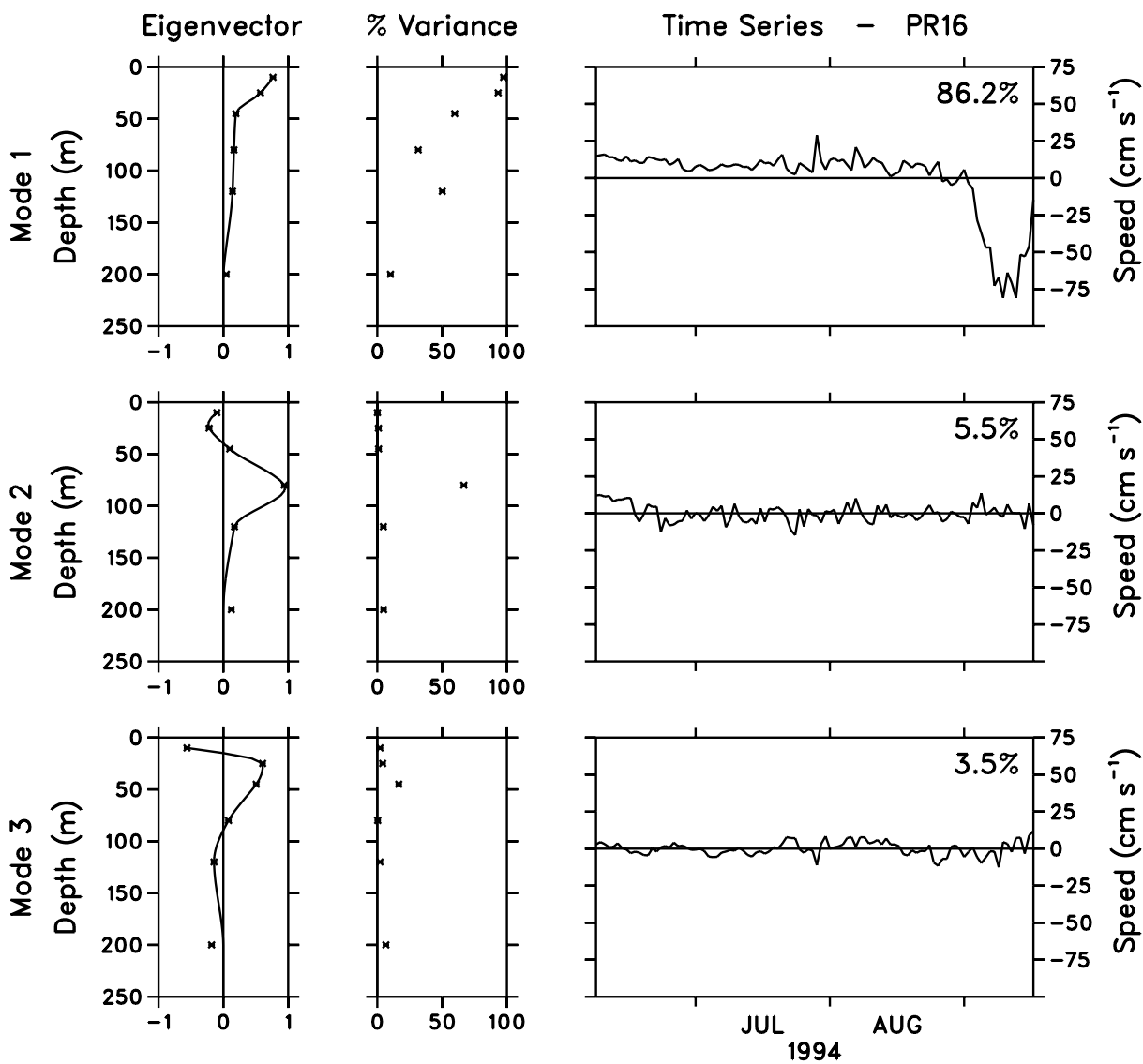


Figure 18: The first three EOF eigenvectors and time series of ADCP-MCM speed differences for PR16. Percent variance explained at each depth is shown in the center panel. Percent of total variance explained by each EOF is shown in the upper right hand corner of the time series panel. The symbols (x) indicate values at individual MCM depths; the solid curve through the individual eigenvector values is a spline fit which has been forced to zero at 200 m.

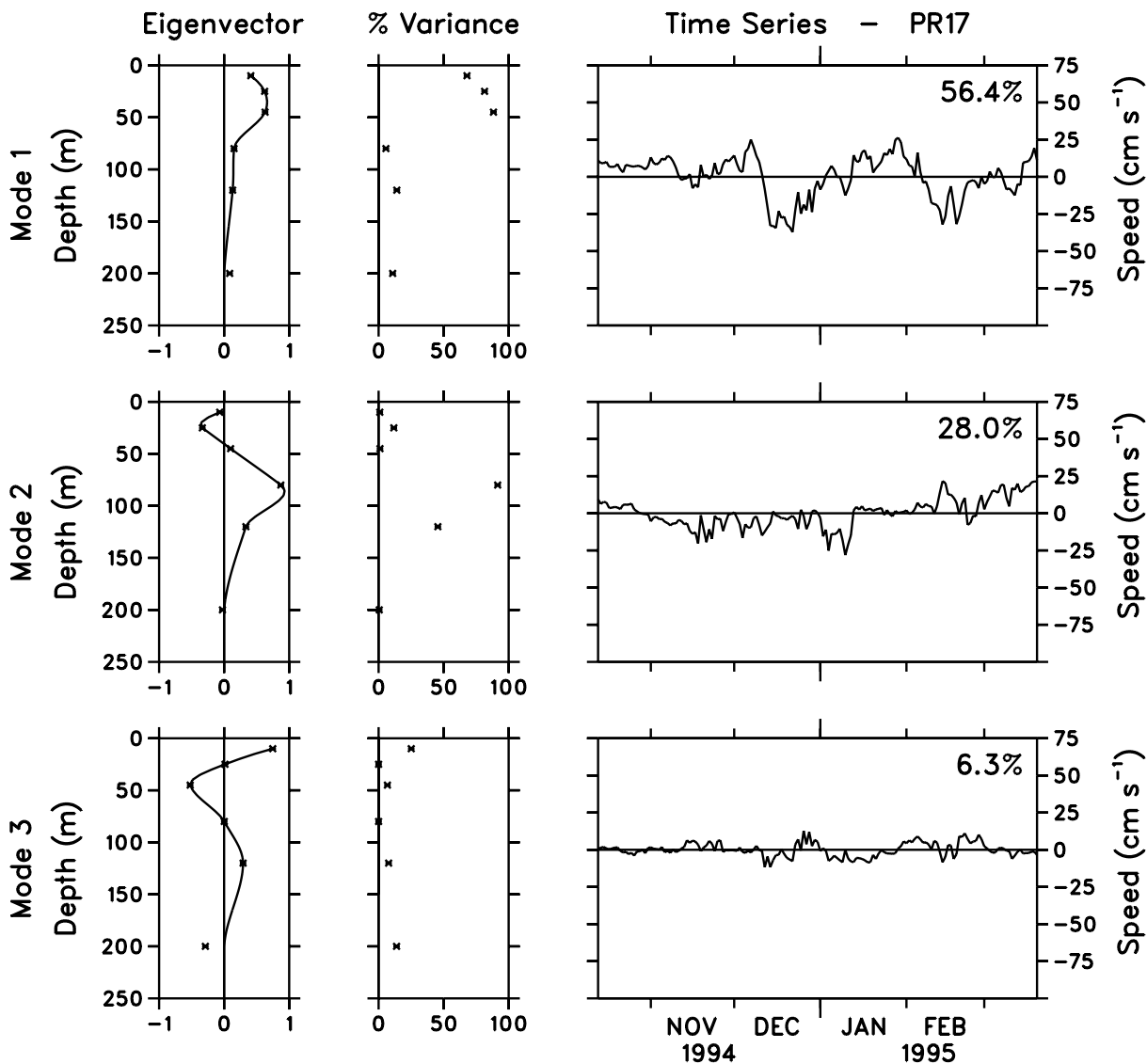


Figure 19: The first three EOF eigenvectors and time series of ADCP-MCM speed differences for PR17. Percent variance explained at each depth is shown in the center panel. Percent of total variance explained by each EOF is shown in the upper right hand corner of the time series panel. The symbols (×) indicate values at individual MCM depths; the solid curve through the individual eigenvector values is a spline fit which has been forced to zero at 200 m.

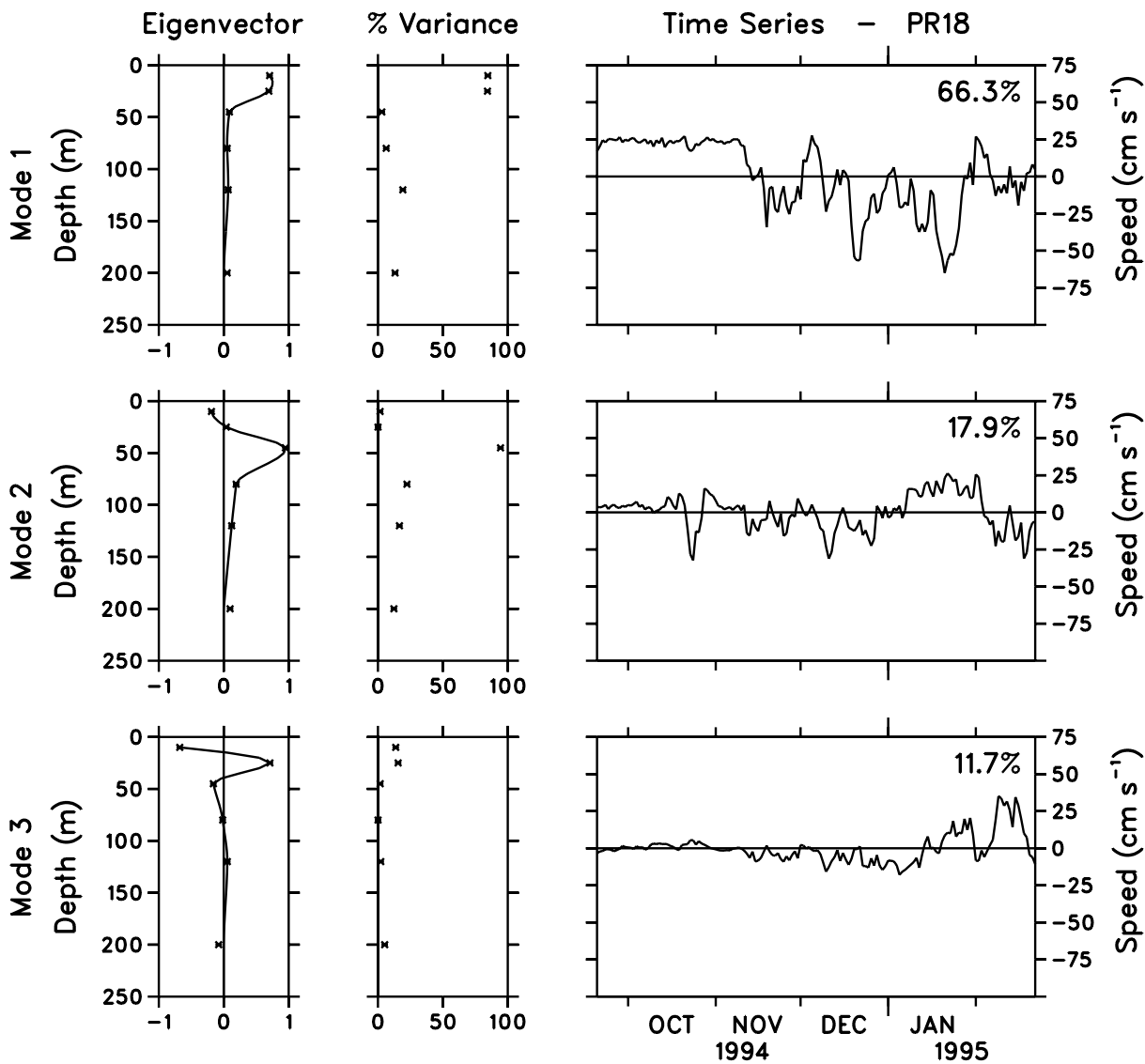


Figure 20: The first three EOF eigenvectors and time series of ADCP-MCM speed differences for PR18. Percent variance explained at each depth is shown in the center panel. Percent of total variance explained by each EOF is shown in the upper right hand corner of the time series panel. The symbols (x) indicate values at individual MCM depths; the solid curve through the individual eigenvector values is a spline fit which has been forced to zero at 200 m.

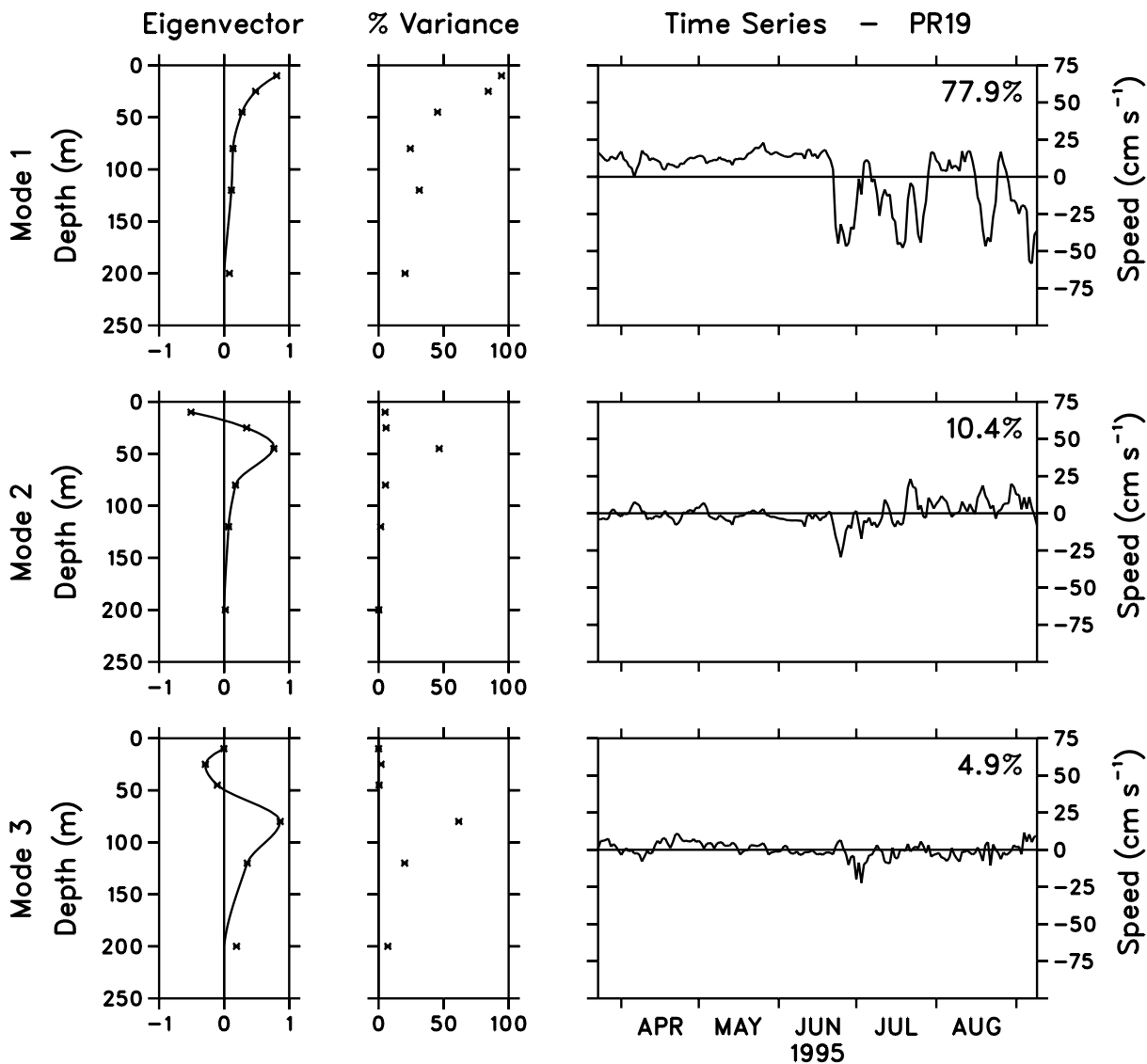


Figure 21: The first three EOF eigenvectors and time series of ADCP-MCM speed differences for PR19. Percent variance explained at each depth is shown in the center panel. Percent of total variance explained by each EOF is shown in the upper right hand corner of the time series panel. The symbols (\times) indicate values at individual MCM depths; the solid curve through the individual eigenvector values is a spline fit which has been forced to zero at 200 m.

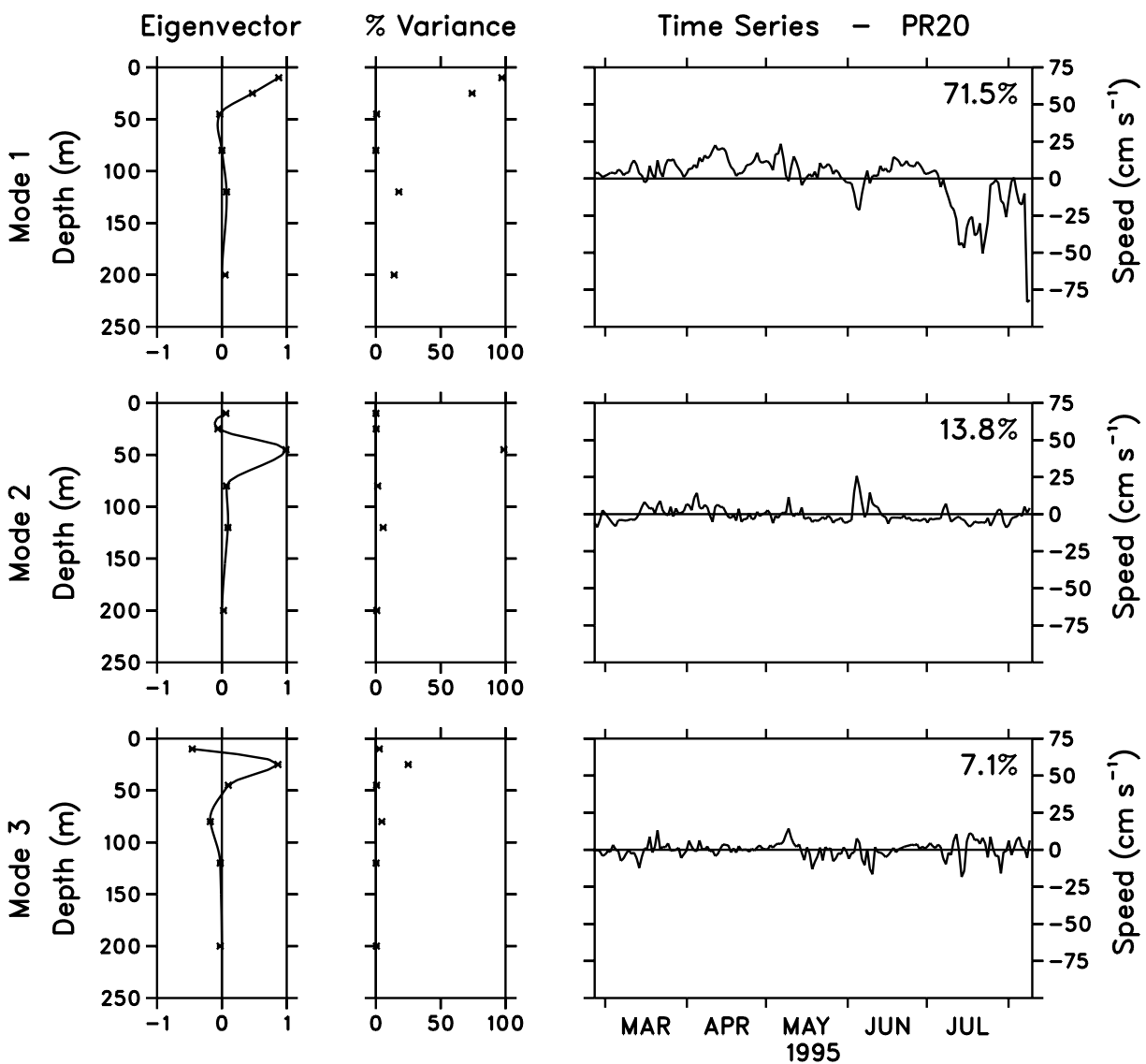


Figure 22: The first three EOF eigenvectors and time series of ADCP-MCM speed differences for PR20. Percent variance explained at each depth is shown in the center panel. Percent of total variance explained by each EOF is shown in the upper right hand corner of the time series panel. The symbols (x) indicate values at individual MCM depths; the solid curve through the individual eigenvector values is a spline fit which has been forced to zero at 200 m.

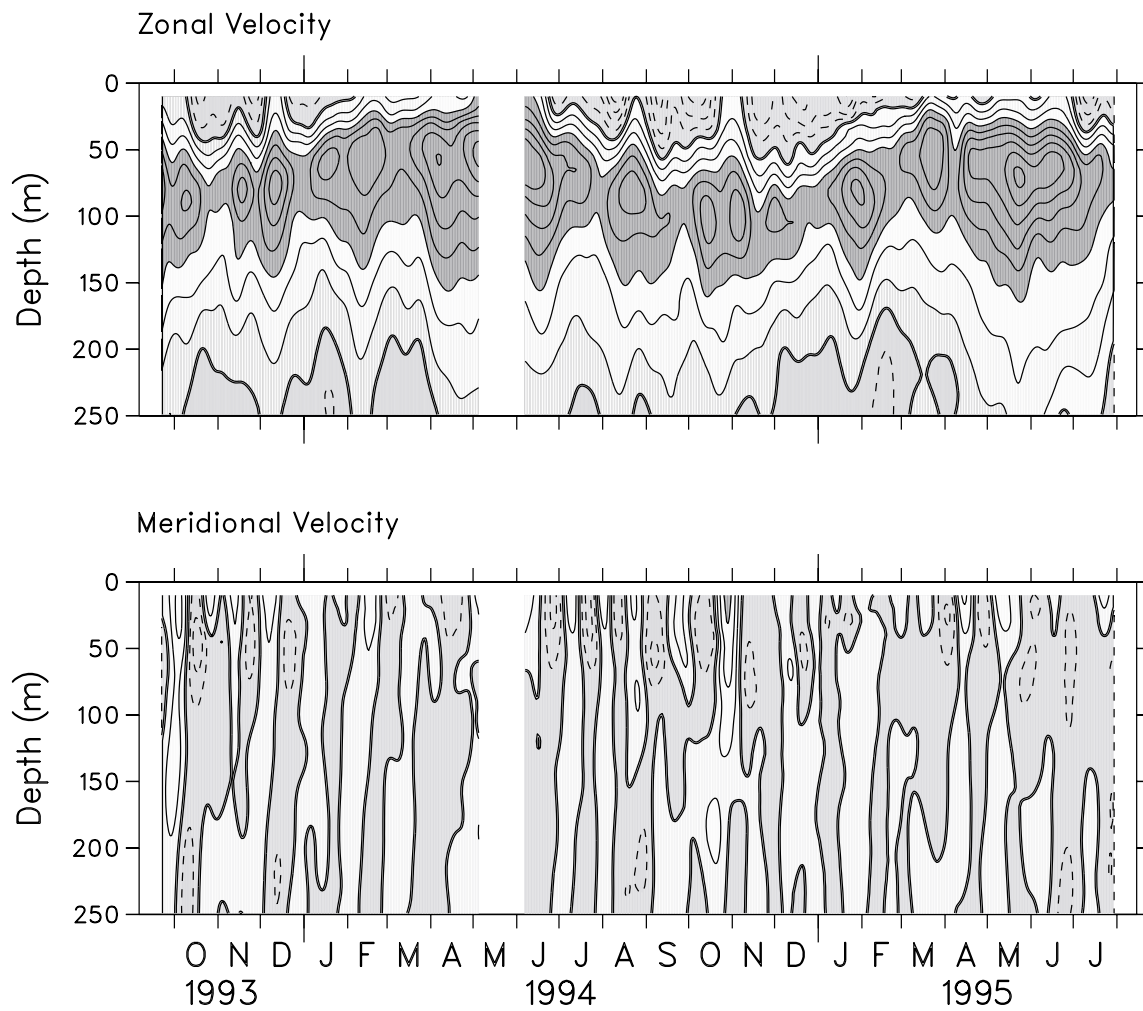


Figure 23: Zonal and meridional velocity at 0° , 110°W from corrected daily profiles of ADCP data. Contours are 20 cm s^{-1} with light shading for westward and southward velocities. Dark shading represents eastward or northward velocities greater than 60 cm s^{-1} .

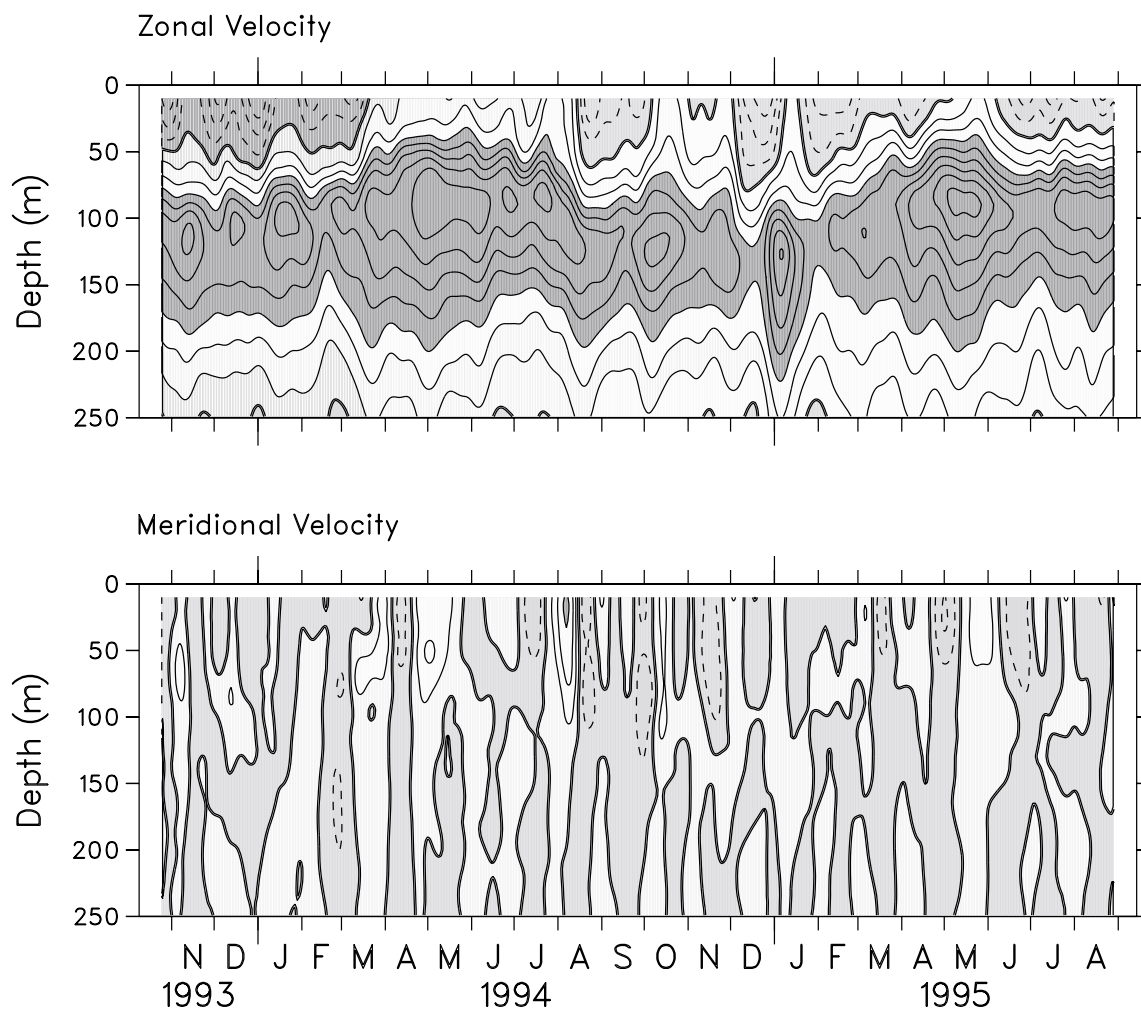


Figure 24: Zonal and meridional velocity at 0° , 140°W from corrected daily profiles of ADCP data. Contours are 20 cm s^{-1} with light shading for westward and southward velocities. Dark shading represents eastward or northward velocities greater than 60 cm s^{-1} .